Environmental Science Nano

ROYAL SOCIETY OF CHEMISTRY

CRITICAL REVIEW

View Article Online
View Journal | View Issue

Cite this: *Environ. Sci.: Nano*, 2025, **12**, 5146

Environmental applications of single-atom nanozymes: recent developments and future directions

Arumugam Selva Sharma [a] and Nae Yoon Lee *[b]

Single-atom nanozymes (SANs) are a new class of artificial enzymes that feature isolated metal atoms anchored to tailored supports. This precise atomic dispersion provides maximum active site utilization while preventing aggregation and leaching, offering enhanced stability and recyclability over traditional nanozymes. This review systematically examines recent advances in the development of SANs for environmental applications, focusing on both pollutant detection and remediation. The review begins with a critical evaluation of synthesis methods of SANs, including pyrolysis, wet chemical, atomic layer deposition, and coordination templating approaches using both carbonaceous and non-carbon supports. Subsequent sections examine the structure–activity relationships governing SANs and describe the factors that modulate their enzyme-like behaviors. Particular emphasis is placed on diverse catalytic properties, with attention to activity-tuning strategies such as heteroatom doping, microenvironmental engineering, and spin-state modulation. Next, the review assesses SANs-based detection platforms, such as colorimetric, fluorescence, electrochemical, and photoelectrochemical systems for monitoring and remediating diverse pollutants. This review critically evaluates current limitations of SANs and outlines strategies for their advancement. Density functional theory (DFT) emerges as indispensable for rational design, enabling computation-guided active site engineering and elucidation of structure–activity relationships. Structurally tunable active centers provide unique opportunities to construct dual-, tri-, and multi-enzyme systems with enhanced catalytic versatility. Future research directions include tandem or bimetallic SANs for multielectron redox catalysis and integrated microdevices combining real-time detection with catalytic mineralization. Particular emphasis is placed on applications where SANs surpass conventional nanozymes or enzymes, thereby establishing design principles for next-generation, multifunctional catalytic platforms.

Received 13th August 2025,
Accepted 16th October 2025

DOI: 10.1039/d5en00750j

rsc.li/es-nano

Environmental significance

Single-atom nanozymes (SANs) have emerged as a novel class of catalysts in which isolated metal atoms are anchored onto support matrices. This structural configuration enables SANs to surpass the catalytic efficiencies of natural enzymes in various applications including environmental monitoring and remediation. In this review, we provide an in-depth survey of various strategies for synthesizing SANs and discuss a range of SANs-based sensing technologies, including optical and electrochemical platforms. Furthermore, we evaluate their effectiveness in the detection and remediation of diverse environmental pollutants, including organic compounds (*e.g.*, phenol, volatile amines, and hydroquinone), pesticides, drug residues, dyes, microbial hazards, and heavy metal ions. The review concludes by outlining future research directions, emphasizing the development of integrated SANs platforms that combine ultrasensitive detection with catalytic degradation, thereby enabling comprehensive "all-in-one" solutions for environmental pollutant management.

Introduction

Natural enzymes exhibit exceptional catalytic performance due to their highly evolved active sites, conformational flexibility, and substrate-specific microenvironments. Their catalytic efficiencies often approach diffusion-limited rates, with precise selectivity and biocompatibility under physiological conditions. However, their inherent fragility such as sensitivity to pH, temperature, and proteolytic degradation combined with high production and purification costs, limits their practical applicability outside biological systems.[1,2] In contrast, conventional nanozymes, comprising

[a] *Department of Nanoscience and Technology, Gachon University, 1342 Seongnam-daero, Sujeong-gu, Seongnam-si, Gyeonggi-do 13120, South Korea*
[b] *Department of BioNano Technology, Gachon University, 1342 Seongnam-daero, Sujeong-gu, Seongnam-si, Gyeonggi-do 13120, South Korea.*
E-mail: nylee@gachon.ac.kr

metal oxides, noble metals, or carbon-based nanomaterials, have emerged as alternatives to their natural enzymatic counterparts. Nanozymes present significant advantages over natural enzymes, including robust structural integrity, cost-effective synthesis, and tunable activity even under harsh chemical conditions. However, their practical efficacy and broader application are hindered by several challenges, namely, inherent structural heterogeneity, low active-site density, and an incomplete understanding of the underlying catalytic mechanisms.[3–5] Moreover, the absence of well-defined active centers allows these nanozymes to act on a broad range of substrates. Nevertheless, this versatility is often accompanied by reduced catalytic specificity and relatively modest turnover efficiency.[6]

Qiao *et al.* demonstrated that a Pt_1/FeO_x single-atom catalyst effectively catalyzed CO oxidation, marking a key advancement in connecting single-atom heterogeneous catalysis with enzyme-like behavior; they also reported that atomically dispersed Pt could achieve turnover frequencies comparable to those of Pt nanoparticles.[7] Applying this single-atom model to nanozymes has subsequently resolved persistent challenges associated with metal/metal oxide-based nanozymes, such as indistinct structure–activity correlations and limited substrate selectivity caused by multiple surface terminations. Consequently, single-atom nanozymes (SANs) have emerged as a transformative class of catalysts in which isolated metal atoms are anchored onto matrices such as M–N–C architectures or graphitic carbon nitride.[8] SANs overcome many of the limitations of natural enzymes and nanozymes as the atom-by-atom dispersion maximizes metal utilization, imposes a well-defined coordination sphere, and facilitates precise electronic modulation.[9] SANs have demonstrated enzyme-mimicking activities including peroxidase, oxidase, and catalase comparable to or exceeding those of both conventional nanozymes and, in some cases, natural enzymes.[1,10] For instance, Fe_3P SANs have shown turnover numbers approaching that of horseradish peroxidase (HRP), along with enhanced durability and recyclability.[1] Moreover, the well-defined electronic structures of SANs create a direct correlation between coordination geometries and favorable kinetic parameters, an advantage intrinsic to natural enzymes but rarely achieved with conventional nanozymes.[11,12]

In recent years, the need for artificial enzymes that exhibit exceptional catalytic specificity has become particularly pronounced in the fields of biosensing and environmental monitoring. For example, colorimetric, chemiluminescence, fluorescence, and electrochemical assays rely heavily on natural redox enzymes, such as horseradish peroxidase or laccase, to generate measurable signals.[13] However, natural redox enzymes denature outside of narrow temperature and pH windows, rendering them unreliable in resource-limited settings. By contrast, SANs can catalyze the oxidation of chromogenic substrates (*e.g.*, 3,3′,5,5′-tetramethylbenzidine (TMB), 2,2′-azino-bis(3-ethylbenzothiazoline-6-sulfonic acid) (ABTS), or luminol) with a turnover several thousand times higher than that provided by metal-oxide nanozymes, enabling sub-micromolar detection of hydrogen peroxide (H_2O_2) and mycotoxins on nitrocellulose membranes or paper without signal drift over weeks of ambient storage.[14,15] Furthermore, SANs typically exhibit greater stability than conventional nanozymes or natural enzymes, particularly under adverse conditions such as elevated temperatures or high salinity. However, the stability of SANs is highly dependent on the specific metal–support system and the coordination environment of the metal atom. All these unique characteristics make SANs well-suited for biological, environmental and marine monitoring applications.[16–19] Moreover, previous studies have demonstrated that atomically dispersed active sites provide nanozymes with excellent catalytic efficacy, which, together with the pronounced environmental

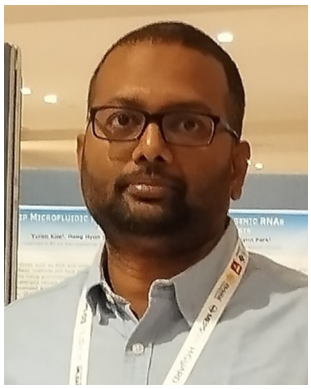

Arumugam Selva Sharma

Dr. Arumugam Selva Sharma received his Ph.D. degree from Bharathiar University, India, in 2016. He conducted postdoctoral research at several institutions, including Pondicherry University, the Sree Chitra Tirunal Institute for Medical Sciences and Technology in India, and Jiangsu University in China, from 2017 to 2023. In 2023, he was appointed as an Assistant Professor at Gachon University in South Korea. His research focuses on developing diagnostic platforms that integrate PCR, LAMP, and nanoparticle-based approaches for colorimetric and fluorometric detection of disease biomarkers and pathogens.

Nae Yoon Lee

Professor Nae Yoon Lee received her Ph.D. degree from the University of Tokyo, Japan in 2004 and worked as a postdoctoral fellow at Korea Advanced Institute of Science and Technology (KAIST) and as a research professor at Ewha Womans University in South Korea from 2004 to 2007. She has been a Professor at the Department of BioNano Technology in Gachon University since 2007. Her main research field is concerned with the development of lab-on-a-chip systems particularly focusing on microdevice fabrication and sealing, surface modification, and developing portable diagnostic devices for point-of-care testing.

stability associated with SANs, is critical for applications in biosensing, environmental monitoring, and food research.[20–22]

Global industrialization, fertilizer-intensive agriculture, and unchecked urbanization have broadly introduced phenolic carcinogens, persistent dyes, antibiotic residues, and heavy metals into air, water, and soil systems. Traditional remediation techniques, such as chlorination, activated sludge, and photocatalysis, often require considerable chemical or energy inputs and generate secondary pollutants. By contrast, SANs activate benign oxidants, such as molecular oxygen, H_2O_2, and persulfate, to generate reactive oxygen species that mineralize contaminants under ambient conditions. In addition to these catalytic degradation capabilities, optical and electrochemical sensors incorporating SANs can measure the heavy metals, organophosphate pesticides, and endocrine-disrupting compounds on flexible platforms at parts-per-billion (ppb) concentrations. When these sensors are embedded within "sense-and-destroy" cartridges, the same single-atom framework can not only quantify the presence of a contaminant but also catalytically eliminate it, thereby integrating detection and remediation into a single operational cycle.[2,23]

Although previous reviews have addressed different aspects of SANs, including synthesis methodologies, surface functionalization, catalytic mechanisms, and biosensing applications, ongoing research continues to reveal new opportunities for the use of SANs in environmental monitoring and remediation.[2,12,14,17,23–29] This review provides an overview of the latest advances in SANs technology, emphasizing optical and electrochemical platforms tailored for pollutant detection and degradation. This review accordingly begins with an in-depth survey of the various strategies for synthesizing SANs with different carbon and non-carbon-based supports as well as the assorted modification strategies used to regulate SAN activity. Subsequently, various SANs-based sensing technologies, including optical and electrochemical platforms, are discussed, and then their effectiveness in the detection and remediation of organic pollutants (phenol, volatile amines, and hydroquinone), pesticides, drug residues, dyes, and heavy metal ions (Scheme 1) is evaluated. Finally, the review concludes by outlining future research directions such as the development of density functional theory (DFT)-assisted synthesis, tandem or bimetallic SANs capable of sequential redox catalysis, and integrated SANs platforms that combine ultrasensitive detection with catalytic degradation to enable "all-in-one" solutions for comprehensive environmental pollutant management.

Literature search and inclusion criteria

Peer-reviewed journal articles on single-atom nanozymes were retrieved from the Web of Science (https://www.webofscience.com/wos/) and CAS SciFinder (https://scifinder-n.cas.org/) databases for publications available prior to August 1, 2025. Keyword searches were conducted using different combinations of words, including "single atom nanozymes", "single atom nanozymes AND environmental applications", "single atom nanozymes AND colorimetric", "single atom nanozymes AND electrochemical", and "single atom nanozymes AND fluorescence". A total of 1429 publications were initially identified. After individual screening to retain only original research articles that specifically focused on the electrochemical and optical detection of environmental pollutants, 80 articles were selected for the review article.

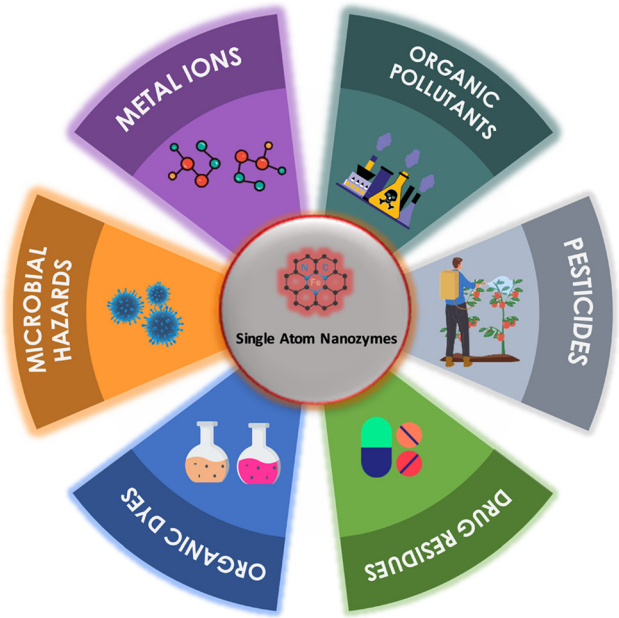

Scheme 1 Overview of SANs in environmental monitoring and remediation applications.

SANs synthesis strategies

The method used to synthesize SANs plays a crucial role in determining their catalytic performance because SANs feature metal centers dispersed at the atomic scale and anchored within well-defined coordination environments. This section accordingly begins with a critical overview of key strategies for synthesizing SANs. Next, various post-synthesis modifications, including ligand exchange, defect passivation, and surface encapsulation, used to fine-tune the catalytic activity and improve the operational stability of SANs, are explored.

Bottom-up synthesis

Wet chemical synthesis. Wet chemical synthesis is the most widely used bottom-up approach for creating SANs. Under this approach, soluble metal precursors are chemically reduced or thermally pyrolyzed in the presence of defect-engineered supports providing lattice vacancies, heteroatom dopants, or extended π-conjugated domains that act as

anchoring sites to capture and stabilize freshly formed metal adatoms. Kim *et al.* immobilized Fe–N_4 motifs within reduced graphene oxide (Fe–N-rGO) to produce SANs that exhibited peroxidase (POD)-like kinetics and applied them to detect H_2O_2 down to concentrations of 10 nM.[30] In another report, Wu *et al.* anchored single Fe atoms on N-doped carbon nanotubes, confirming atomic dispersion by extended X-ray absorption fine structure (EXAFS) and achieving four-fold higher POD-like activity than commercial Fe_3O_4 nanozymes.[31] Notably, although wet chemical synthesis protocols offer a low-temperature, scalable approach, the resulting metal loadings seldom exceed ~2 wt%. Moreover, the presence of residual capping ligands often blocks the catalytically active centers in wet chemical synthesized SANs.

Atomic layer deposition. Atomic layer deposition (ALD) operates through a self-limiting, sequential surface chemistry in which each precursor exposure deposits at most one atomic layer, thereby affording angstrom-level control over film thickness and composition. Sun *et al.* used ALD to deposit single isolated Pt atoms on graphene, doubling the mass activity for the oxygen-reduction reaction relative to that of conventional Pt nanoparticle catalysts (Fig. 1A).[32] More recently, Zhou *et al.* employed ALD to graft isolated Rh atoms onto SnO_2 by pulsing tris(acetylacetonato)-rhodium and O_2 at 200–250 °C for two cycles to deposit ~0.05 wt% Rh sub-monolayers. The resulting single-atom film exhibited excellent catalytic kinetics and gas-sensing selectivity performance.[33] Although ALD offers angstrom-scale control, the need for vacuum hardware and long cycle times can hinder large-volume environmental applications of this technology.

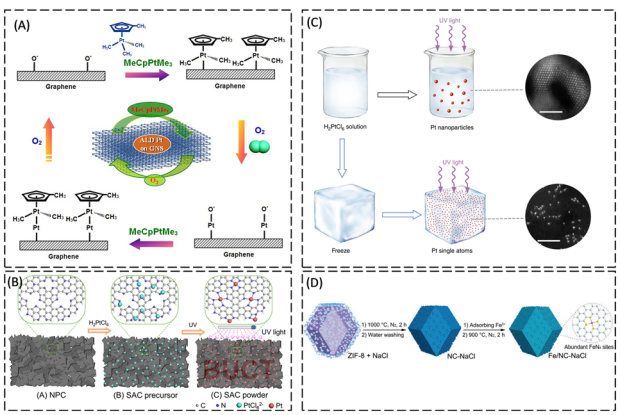

Fig. 1 (A) Schematic representations of the Pt ALD mechanism over graphene nanosheets, reproduced with permission from ref. 32, Copyright 2012 Springer Nature, (B) schematic diagram of the synthesis process for the Pt_1/NPC catalyst, reproduced with permission from ref. 34, Copyright 2018 American Chemical Society, (C) schematic depiction of the iced-photochemical process, reproduced with permission from ref. 35, Copyright 2017 Springer Nature, and (D) schematic representation of the Fe/NC–NaCl preparation process employing surface–molten NaCl. The molecular visualization uses gray (C), yellow (N), and pink (Fe) spheres to denote the respective atoms, reproduced with permission from ref. 41, Copyright 2021 John Wiley and Sons.

Photochemical synthesis. The photochemical synthesis strategy employs ultraviolet (UV) photons (often at subzero temperatures) to reduce adsorbed metal complexes and suppress thermal diffusion that would otherwise form clusters during the preparation of SANs. Li *et al.* employed a photochemical solid-phase reduction strategy to anchor atomically dispersed Pt onto N-doped porous carbon (Pt_1/NPC), obtaining a metal loading of 3.8 wt% and achieving a 24-fold increase in activity compared with that of commercial Pt/C (Fig. 1B). Spectroscopic observations indicated that this markedly enhanced electrocatalytic performance was predominantly a result of a well-defined Pt–N_4 coordination environment established by electron transfer from the isolated Pt centers to adjacent N atoms.[34] Wei *et al.* reported a photochemical strategy in which cryogenically frozen H_2PtCl_6 was irradiated to yield atomically dispersed Pt on mesoporous carbon and TiO_2, conferring a high oxidation activity relative to commercial Pt/C catalysts (Fig. 1C).[35] Notably, photochemical processes have attracted renewed interest for low-carbon catalyst manufacture because they are ligand-free and energy-efficient.

High-energy ball milling. High-energy ball milling has emerged as a versatile and solvent-free method for generating atomically dispersed metal sites on defect-rich supports. Gan *et al.* developed a scalable dry ball milling method for the large-scale synthesis (>1 kg) of single-atom Au_1/CeO_2 catalysts. The resulting Au_1/CeO_2 exhibited exceptional catalytic performance for the preferential oxidation of CO at 120 °C, achieving complete CO conversion (100%) with high selectivity and stability. Kinetic studies revealed that the turnover frequencies for H_2 oxidation over Au_1/CeO_2 at 120 °C (<0.01 s^{-1}) were approximately two orders of magnitude lower than those for CO oxidation, demonstrating a practical and scalable route for manufacturing high-performance SACs with uniform reactivity.[36] Extending this concept, Xu *et al.* developed a two-stage ball milling method in which N-doped carbon (5.0 g) and metallic Cu powder (100 mg) were co-milled in a 70 mL iron jar containing thirty 6 mm agate balls at 100 W for 6 h to produce a CuNP–NC composite. This composite (5.0 g) was subsequently subjected to a second 6 h milling cycle under identical conditions to further reduce the particle size and enrich the defect sites capable of binding single atoms. Finally, the milled material was subjected to an acid etching treatment for 1 h, washed with water, and then dried at 80 °C overnight to yield Cu-anchored N-doped carbon (Cu–NC) SANs. These SANs exhibited nearly twice the POD-like activity of CuNP–NC owing to improved H_2O_2 activation. This enhanced efficiency makes Cu–NC SANs promising candidates for applications in catalysis and oxidative reactions.[37]

Mass-selected soft-landing synthesis. The mass-selected soft-landing synthesis strategy offers control over nuclearity and charge states when depositing metal species onto supports. Heiz *et al.* generated size-filtered Pt_{1-n} clusters (where n = 1–30) in a gas-phase source. These clusters were subsequently deposited onto a clean MgO (100) surface after

momentum softening to form atomically precise, ligand-free Pt ensembles. The researchers systematically mapped the catalytic activities of these Pt_{1-n} ensembles in CO oxidation, revealing direct correlations between the cluster structure and reactivity.[38] Furthermore, Kwon *et al.* deposited mass-selected Pt_7 and Pt_9 clusters onto ultrathin Al_2O_3 films in an ultra-high vacuum, achieving sub-monolayer coverage with angstrom-level spatial precision. Operando X-ray absorption and DFT analyses revealed size-dependent d-band modulation, which translated into order-of-magnitude enhancements in the ethylene hydrogenation turnover frequencies of the Pt clusters relative to those of bulk Pt.[39]

Top-down synthesis

In contrast to bottom-up synthesis methods, top-down synthesis methods systematically split bulk metals or preformed nanoparticles into discrete single-atom sites through chemical etching and electrochemical stripping. The liberated metal atoms subsequently migrate toward the heteroatom dopants or intrinsic lattice defects, where they anchor firmly. These robust metal–support interactions inhibit agglomeration and leaching, thereby imparting exceptional structural integrity and long-term catalytic durability to the resulting materials.

High-temperature pyrolysis and gas-phase migration. High-temperature pyrolysis is a powerful top-down method for generating isolated single-atom sites. Under this method, metal–organic frameworks (MOFs) or zeolitic imidazolate frameworks (ZIFs) serve as nitrogen-rich sacrificial templates for fabricating SACs. Fan *et al.* encapsulated Fe-ZIF-8 crystals within a SiO_2 shell, subjected this core–shell architecture to pyrolysis at 900 °C, and then removed the silica layer to expose atomically dispersed Fe sites. The transient SiO_2 barrier effectively inhibited Fe agglomeration during carbonization, yielding an SAC exhibiting four times more POD-like activity than its uncoated counterpart.[40] Wang *et al.* utilized molten NaCl as a spatial-confinement medium to encapsulate an Fe–Zn ZIF precursor during 900 °C pyrolysis. The NaCl melt suppressed metal sintering, producing a high-density array of Fe–N_4 sites (3.2×10^{19} sites g^{-1}) that retained >95% catalytic turnover in 0.1 M HCl, reflecting exceptional acid resistance (Fig. 1D).[41] In another study, Liu *et al.* synthesized a self-supporting Co–N–C catalyst featuring exclusively single-atom dispersed Co sites using a sacrificial support strategy. This approach initially deposited a Co(II) bis(1,10-phenanthroline) diacetate precursor on a $Mg(OH)_2$ support. The resulting composite material subsequently underwent pyrolysis at 700 °C in a N_2 atmosphere for 2 h. Following thermal treatment, the sacrificial MgO template was selectively etched using nitric acid treatment, yielding the final catalyst with a well-defined atomic dispersion of Co species within the N-doped carbon matrix. This structurally defined catalyst demonstrated exceptional performance in the chemoselective hydrogenation of nitroarenes to azo compounds under mild conditions.[42]

Among all the preparation methods discussed, pyrolysis remains the most extensively adopted technique for gram-scale synthesis.[43] Pyrolysis of MOFs, such as ZIF-8, allows effective confinement of metal ions during high-temperature treatment, resulting in high-density single-atom dispersion.[43] This method is scalable and already demonstrates gram-level output in laboratory settings with relatively high reproducibility when key parameters such as temperature, ramp rate, and inert atmosphere are strictly controlled.[8,44] However, challenges still remain such as metal atom aggregation and uneven thermal distribution which limit its scale-up toward kilogram levels.[45] Ball milling, a solvent-free and energy-efficient method, is increasingly favoured due to its eco-friendly profile. It has shown potential for kilogram-scale synthesis and offers a green and reproducible route for preparing SANs with well-dispersed atomic sites, especially when combined with post-annealing steps.[36,46] Control over mechanical parameters (*e.g.*, milling speed and ball-to-powder ratio) is essential to achieve uniformity and reproducibility across batches.[17] Wet-chemical methods offer moderate scalability and simplicity but often suffer from limited control over the coordination environment and require post-treatment steps (*e.g.*, calcination or ligand removal), which can compromise atom dispersion and reduce batch reproducibility.[17] In contrast, atomic layer deposition (ALD) provides precise atomic control and high reproducibility by sequential self-limiting surface reactions. However, the low throughput and high operational cost of ALD hinder its suitability for large-scale production of SANs unless adapted into more scalable configurations.[43,47] At present, pyrolysis and ball milling represent the most promising synthesis approaches for scalable and sustainable preparation of SANs. While ALD and wet-chemical methods offer advantages in precision, their scalability remains constrained. Continued efforts toward process optimization, precursor engineering, and green synthesis will be essential to bridge the gap between laboratory synthesis and industrial applications of SANs.

Carbon- and non-carbon-based supports

The presence of isolated active centers in a SANs depends on the physicochemical properties of the host support. Nitrogen-rich carbon support architectures, such as graphene, carbon nanotubes, graphdiyne, and MOF-derived N-doped carbon, provide exceptionally high specific surface areas. Furthermore, their abundant heteroatom coordination motifs ($M–N_x$) secure individual metal atoms and modulate the d-band electronic structure, thereby contributing to improved enzyme-like catalytic turnover. Choi *et al.* developed an S-doped zeolite-templated carbon support featuring a three-dimensional (3D) graphene nanoribbon network and high S content (17 wt%) that enabled exceptional Pt dispersion (5 wt%) as isolated atoms and clusters. Remarkably, this catalyst selectively produced H_2O_2 *via* a two-electron oxygen reduction pathway, maintaining sustained activity without

degradation, in contrast to conventional four-electron reduction to H_2O. Indeed, its unique carbon architecture and S-doping synergistically stabilized Pt species, offering a promising route for sustainable H_2O_2 production.[48]

Cheng *et al.* designed carbon nanotube-supported SANs (CNT/Fe–N–C) featuring atomically dispersed Fe–N_x active sites and synthesized them using NaCl crystals as sacrificial templates. The π–π stacking of Fe–N_x motifs between nanotube walls further decreased the Michaelis constant for H_2O_2 activation (0.129 mM for CNT/Fe–N–C SANs *vs.* 0.241 mM for Fe_3O_4 nanozymes), demonstrating the acceleration of electron transfer *via* conductive carbon.[49] Furthermore, the use of MOFs can exploit strong metal–support interactions. For example, single Pt atoms on CeO_2 coupled their 5d orbitals with Ce 4f states, considerably enhancing radical-scavenging efficacy in neuro-injury models.[50] Likewise, Co nanodiscs anchored on phase-distorted 1 T-MoS_2 reconfigured the sulfide lattice and synergistically boosted POD-like catalysis beyond that of either component alone.[51]

Thus, optimal SANs designs depend on three parameters: (i) anchoring energy, which prevents sintering, (ii) electronic coupling, which tailors adsorption energetics, and (iii) transport architecture, which maximizes substrate flux.[2] Carbonaceous matrices excel in providing conductivity and heteroatom tunability and are well-suited for use in electrochemical biosensors as a result, whereas reducible oxides and chalcogenides provide strong metal–support interactions for the oxygen-based chemistries integral to pollutant degradation. Therefore, rational metal–support pairing is critical to achieving improved SANs performance across bioanalytical, therapeutic, and environmental applications.

Modification strategies for regulating the activity of SANs

Heteroatom-directed microenvironment engineering and spin-state modulation have emerged as potent control for regulating post-synthesis activity in SANs. Remote heteroatom doping provides powerful electronic modulation without sacrificing site isolation. Indeed, the insertion of P into Fe–N_4 motifs on carbon nanowires redistributed charge at the metal center and tripled the POD-like turnover frequency at 25 °C.[52] By contrast, B donation reduced the activation barrier for hydroxyl radical generation, thereby accelerating chromogenic TMB oxidation.[53] Furthermore, F-doped Fe–N–C SANs exhibited enhanced CO_2 electroreduction performance owing to the electron-withdrawing effect of F, which stabilizes Fe^{3+} active sites.[54] Besides first-shell chemistry, tailoring the coordination number and spin state affords another degree of freedom. A five-coordinated FeN_5 site prepared by controlled ligand addition generated six times more hydroxyl radicals than the canonical Fe–N_4 analog, translating into superior tumor ablation in murine models.[55] Conversely, lowering the spin of Fe–N_4 centers to match that of natural catalase eliminated radical overproduction, enabling non-cytotoxic intracellular H_2O_2 scavenging.[56]

At the support level, the insertion of single Ni atoms into S-vacancy-rich MoS_2 accelerated interfacial charge transfer and realized dopamine sensing down to 0.2 nM, two orders of magnitude below that realized by pristine dichalcogenide.[57] Under harsh conditions, thermodynamic mobility of metal atoms leads to deactivation dominated by Ostwald ripening, ligand leaching, and support corrosion. To address this challenge, current stabilization strategies focus on complementary approaches, including enhancing metal–support interactions through high-energy M–N or M–O covalent bonds (2 eV), embedding atoms within thermally robust carbon nanoframes or silica shells (stable up to 900 °C), and employing redox-active "self-healing" matrices to restore migrated atoms to their original states. Nevertheless, no single strategy has ensured continuous operation beyond 1000 h under combined acidic and saline conditions, highlighting the importance of SANs stability for practical applications.

However, recent research work has been expanding the notion of catalytically "active sites" from strictly isolated atoms to correlated atomic assemblies that balance high turnover frequencies with enhanced stability. For example, diatomic SANs comprising Fe–Se pairs embedded in a carbon matrix have simultaneously accelerated oxygen reduction and peroxide decomposition, increasing the specific power of neutral Zn–air batteries by approximately 30%.[58] Furthermore, dual-metal or trimeric constructs, such as Ni(Co)–Ru–P clusters synthesized by gradient atomic layer deposition, have achieved near-unity faradaic efficiency in H_2N_4 dehydrogenation to power self-driven H_2 generators.[59] Thus, by uniting atomic-precision synthesis, micro-environment regulation, and durability assurance, next-generation SANs have the potential to become low-cost, high-performance materials for environmental monitoring and green catalysis.

Structure–activity relationships and factors influencing the enzyme-like activities of SANs

The nanozyme and catalytic efficacy of SANs are intrinsically governed by their metal coordination environment and electronic structure. A central factor influencing catalytic efficiency in SANs is the identity and coordination structure of the metal active center.[10,60,61] Recent studies underscored that Fe–N_4, Co–N_4, and Mn–N_X active sites embedded within nitrogen-doped carbon substrates facilitate divergent reactive oxygen species (ROS) generation pathways, depending upon their electronic configuration, ligand field, and interaction with reaction mediators (H_2O_2).[1,62] Metal–nitrogen motifs such as Fe–N_4, Co–N_4, and Mo–N_x have shown distinct reactivities depending on the coordination number and electronic structure of the metal atom.[6,63] For instance, a

comparative study of M–N_4 sites (M = Fe, Co, and Zn) revealed that Fe–N–C SANs exhibit superior POD-like activity, as evidenced by enhanced signals in electron paramagnetic resonance (EPR) indicating higher generation of hydroxyl radicals. DFT calculations attributed this superiority to favorable electron transfer properties and optimized adsorption energetics. Specifically, the d-band center of Fe–N–C (−1.40 eV) was closer to the Fermi level than those of Co–N–C or Zn–N–C analogues, facilitating stronger interactions with intermediates and promoting H_2O_2 activation. This underscores the critical role of the electronic structure of the metal center in determining catalytic performance.[64] The catalytic performance of SANs is driven by the surrounding ligand numbers and species. For instance, a ligand engineering strategy applied to Pt-based SANs transformed Pt–N_4 into a Pt–N_3PS structure. Although H_2O_2 binding affinity remained largely unchanged due to the similar carbon support, the altered electronic structure such as inverse Bader charge and modified charge density of the Pt–N_3PS site shifted the free-energy of the reaction pathway. This electronic redistribution resulted in a higher turnover number and greater POD-like catalytic efficiency compared to the conventional Pt–N_4 configuration.[24,65]

The electronic structure and geometry of the metal center in SANs govern the energy profile of the reaction pathway. Consequently, these structural parameters directly determine the identity of the rate-determining step (RDS) by influencing the adsorption energies of key intermediates and the activation barriers for critical events such as bond cleavage and electron transfer. As a key indicator of catalytic performance, the RDS not only governs the overall reaction kinetics but also controls the selectivity of ROS generation. This structure–activity relationship is clearly demonstrated by the distinct RDS behaviors observed across different metal–N_x configurations. For conventional Fe–N_4 motifs, the RDS in POD-like catalysis typically involves the transformation of surface hydroxyl species derived from H_2O_2 dissociation, such as the 2OH → O + H_2O step, which carries a relatively high barrier (~1.05 eV).[66] In contrast, the engineered FeN_3P coordination environment, where one nitrogen atom is replaced by phosphorus, significantly lowers this barrier. DFT calculations and XAFS analyses showed that P coordination modifies the local electronic structure, reduces electron withdrawal from the Fe center, and facilitates electron donation *via* a P → Fe → N pathway. As a result, the FeN_3P site achieves lower activation barriers for O and OH formation (<0.5 eV), enhanced stabilization of reactive intermediates, and a shift in the RDS from sluggish OH conversion on Fe–N_4 to a much easier O migration step on FeN_3P. This modulation of orbital overlap and charge distribution at the Fe center rationalizes the observed 10-fold increase in catalytic activity compared to Fe–N_4 analogues.[1] A study by Xu *et al.* showed that the design of a cobalt single-atom nanozyme can directly affect and improve the rate-determining step (RDS) in OXD-like catalysis. A concave carbon framework with many edge Co–N_4 sites was constructed, and this changes the electronic state of the cobalt center. In this way, the catalyst has stronger interaction with oxygen, which makes the adsorption and activation of O_2 easier. Theoretical calculation also confirms that this structure lowers the activation energy of the RDS, which is usually the first oxygen splitting step. Due to this decrease, the catalytic activity becomes 3.1 times higher. This finding shows a clear relationship between the structure and performance, and gives useful guidance for future nanozyme design.[67]

The catalytic activity and ROS selectivity of SANs are highly sensitive to environmental pH, salinity, and radical scavengers significantly. This in turn directly influences metal valence states, substrate adsorption, and reaction pathways. For example, Fe–N–C SANs exhibit maximal POD-like activity under acidic conditions (pH ≈ 3–4), where low pH facilitates favorable Fe(III)/Fe(II) redox cycling and enhances H_2O_2 activation.[66] However, such acidic dependence limits practical applications. To address this limitation, coordination engineering has been employed. Huang *et al.* demonstrated that in Co-based SANs, reducing the nitrogen coordination number (*e.g.*, Co–N_2) shifts the catalytic mechanism toward a singlet oxygen ($^1O_2$)-dominated non-radical pathway. This pathway maintains high efficiency over a broad pH range between 3 and 9, as it avoids pH-sensitive radical generation and instead relies on stable electronic configurations less affected by proton concentration.[68] Such structural design strategies effectively decouple catalytic performance from acidic conditions, thereby enhancing the practicality of SANs for environmental applications. The presence of halide ions (*e.g.*, Cl^- and Br^-) in saline environments introduces competitive adsorption and leads to the formation of reactive halogen species, which can further alter the dominant ROS pathway.[69] Radical scavenging experiments provide key insights into reaction mechanisms. For example, if catalytic activity continues when sodium azide (a known singlet oxygen, $^1O_2$, quencher) is added, but ceases when isopropanol (a hydroxyl radical scavenger) is introduced, this strongly indicates a non-radical mechanism in which $^1O_2$ is the primary reactive species.[70] Such a non-radical mechanism is frequently observed in Co–N_4 nanozymes.[71]

Enzyme-like properties of SANs

SANs exhibit multispecies enzymatic activity including POD-like, superoxide dismutase (SOD)-like, oxidase (OXD)-like and catalase (CAT)-like functionalities, often demonstrating multiple activities simultaneously. The following section provides a focused discussion on the major enzyme-like activities of SANs. In particular, it examines the mechanisms and applications of their POD-like, SOD-like, OXD-like and CAT-like properties. A comprehensive understanding of these properties is critical, as it provides insights into the catalytic mechanisms inherent to SANs and helps with the rational

design for practical applications in fields such as biosensing, biomedicine, and environmental remediation.

Peroxidase (POD)-like activity

POD-like behaviour is the most widely studied enzymatic function of SANs. In this mechanism, H_2O_2 is decomposed into highly reactive hydroxyl radicals that oxidize organic substrates such as TMB, diazoaminobenzene (DAAB), and *o*-phenylenediamine (OPD). In natural peroxidases such as HRP, the catalytically active center consists of a porphyrin-bound iron cofactor, in which the Fe atom is coordinated with four nitrogen atoms on the porphyrin ring plane.[2,72] This structural motif provides the fundamental inspiration for designing Fe-based single-atom materials to emulate the enzymatic active site. For instance, Fe–N–C SANs obtained *via* high-temperature pyrolysis of MOFs have been successfully applied to biosensing, including the detection of butyrylcholinesterase (BChE) activity.[73] Similarly, Wang and co-workers developed Fe-SA/NC catalysts and employed them in a ratiometric fluorescence sensing platform for acetylcholinesterase (AChE) activity, demonstrating the adaptability of POD-like SANs to diverse biosensing applications.[74] Besides iron, other transition metals have been explored to replicate or extend POD-like activity. Recent studies have focused on molybdenum-based SANs, where systematic modulation of the coordination environment has been used to tune catalytic behavior. A representative example is the Mo–N_x–C series, synthesized by pyrolyzing Mo-ZIF-8 MOFs supported on N-doped porous carbon. These materials were evaluated through the colorimetric oxidation of TMB at 652 nm, a classical peroxidase assay. Among the series, Mo–N_3–C exhibited the highest POD-like activity. Advanced spectroscopic techniques such as X-ray absorption fine structure (XAFS) analysis revealed that the number of nitrogen ligands coordinating the Mo center played a decisive role in dictating peroxidase specificity and catalytic efficiency (Fig. 2A).[75] The atomically dispersed M–N–C motifs not only reproduce the spatial and electronic features of enzyme cofactors but also provide opportunities for rational modulation of activity through careful control of the metal type and coordination environment.

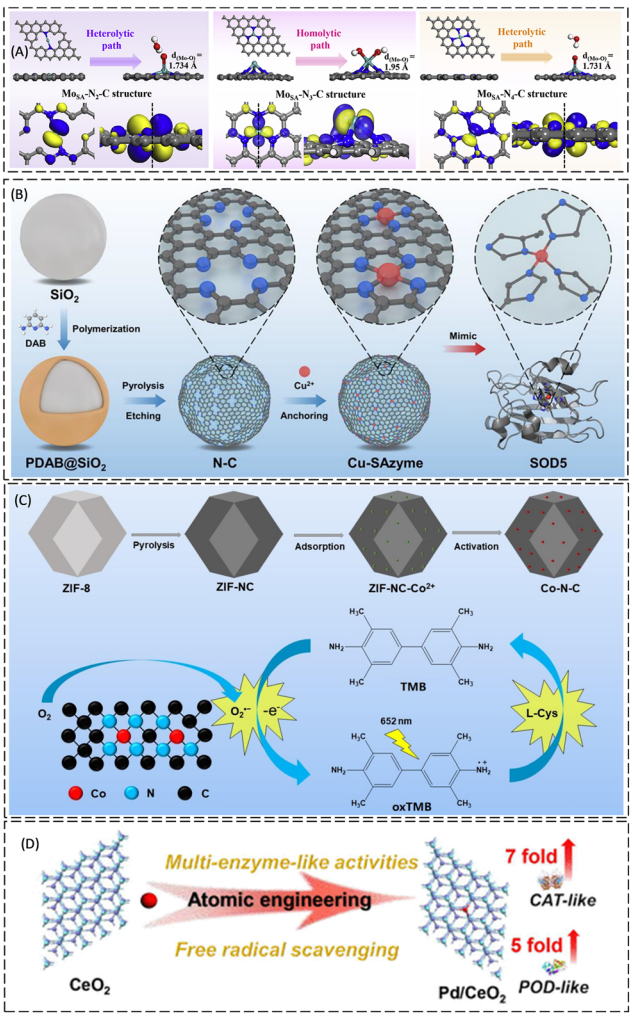

Fig. 2 (A) Schematic showing the theoretical investigation of the mechanism for the coordination number-dependent POD-like specificity of Mo–N_x–C SANs, reproduced with permission from ref. 75, Copyright 2020 Elsevier Inc. (B) Scheme showing the synthesis of Cu-SANs with SOD-like activity, reproduced with permission from ref. 76, Copyright 2025 John Wiley and Sons. (C) Schematic depicting the synthesis of Co–N–C SANs and their OXD-like activity in enabling the colorimetric detection of L-cysteine, reproduced with permission from ref. 79, Copyright 2025 Elsevier Inc. (D) Schematic showing the activity increment of Pd/CeO_2 SANs, reproduced with permission from ref. 82, Copyright 2022 American Chemical Society.

Superoxide dismutase (SOD)-like activity

SOD-like activity represents a crucial antioxidant function of SANs, enabling the dismutation of superoxide anions into oxygen and H_2O_2. This property is commonly evaluated through colorimetric assays, such as the riboflavin–nitro blue tetrazolium (NBT) or WST systems, where the reduction of tetrazolium salts into chromogenic formazan provides a quantifiable measure of activity at 560 or 450 nm, respectively.[2,72] A broad range of SANs incorporating metals such as Mn, Pt, Au, Ni, Cu, Fe, Rh, Mo, and Co have demonstrated SOD-mimicking behavior, but copper-based systems have received particular attention owing to their structural analogy to natural Cu-only SOD enzymes. For instance, Cu–N_4 SANs were shown to effectively scavenge superoxide radicals in sepsis models, thereby interrupting reactive oxygen and nitrogen species (RONS)-mediated inflammatory cascades and improving multi-organ outcomes, underscoring their therapeutic potential in critical care (Fig. 2B).[76] Similarly, bimetallic designs such as Cu/Zn single-atom nanozymes have been developed to structurally resemble natural Cu/Zn-SOD, demonstrating selective and highly efficient scavenging of superoxide anions with catalytic activities (7820 U mg^{-1}), surpassing those of natural SOD, while avoiding unwanted POD or OXD-like reactions.

This selectivity, coupled with low toxicity and stability against aggregation, highlights the advantages of single-atom approaches over conventional nanoceria systems.[77]

Oxidase (OXD)-like activity

OXD-like properties are another crucial enzymatic mimicry observed in SANs. Unlike POD-like activity, which depends on H_2O_2, OXD-like catalysis involves the direct reduction of oxygen to reactive intermediates, enabling substrate oxidation in the absence of external oxidants.[2,72,78] Transition-metal–nitrogen–carbon frameworks, particularly those containing Fe, Co, or Ni centres, have demonstrated strong OXD-like activity.[2,72] The underlying mechanism often follows a ping-pong pathway, where electron transfer occurs sequentially between the substrate, the metal site, and molecular oxygen. For instance, cobalt-based Co–N–C SANs derived from ZIF-8 precursors have demonstrated remarkable OXD-like activity, catalyzing the oxidation of TMB into a chromogenic product, oxTMB, which serves as the basis of a highly sensitive and selective colorimetric platform for L-cysteine detection (Fig. 2C).[79] Similarly, rational engineering of Fe–N–C SANs with densely exposed FeN_4 sites on hierarchical porous carbon supports has significantly enhanced intrinsic OXD-like activity by modulating the electronic structure of iron centers through edge effects. These optimized Fe–N–C systems achieved superior catalytic kinetics in TMB oxidation and were successfully applied in uric acid detection.[80] In another study, boron–nitrogen co-doped Zn-based SANs (ZnBNC-SANs) were developed with finely tuned Zn–N–B coordination environments that shifted the electronic band structure to promote OXD-like catalysis. These ZnBNC-SANs formed the basis of an advanced RNA sensing platform independent of H_2O_2, integrating CRISPR/Cas13 technology with DNA extension reactions to achieve ultra-sensitive detection as low as 20 aM.[81] These studies suggest that the rational design of the atomic coordination environment is a critical determinant of catalytic function. By precisely engineering Co-, Fe-, and Zn-based single-atom centers, powerful OXD-like SANs can be realized, offering broad potential for advancing fields such as biosensing, clinical diagnostics, and point-of-care testing.

Catalase (CAT)-like activity

CAT-like activity in SANs involves the disproportionation of H_2O_2 into water and molecular oxygen, thereby preventing harmful peroxide accumulation. SANs with atomically dispersed $Fe–N_4$ sites synthesized *via* high-temperature pyrolysis have demonstrated dual CAT- and SOD-like functions, effectively reducing electron spin resonance signals generated by superoxide radicals and confirming their intracellular ROS-scavenging potential.[56] In another report, Pd/CeO_2 SANs prepared through a simple aqueous method exhibited superior catalytic efficiency, with 3 to 7-fold higher CAT-like activity compared with conventional CeO_2 nanozymes, highlighting the synergistic advantages of atomic dispersion and strong metal–support interactions (Fig. 2D).[82] Even greater enhancements have been achieved through rational coordination engineering. For instance, L-cysteine-activated Cu–MoO_x SANs (MCCP SANs) displayed a CAT-like catalytic efficiency 138 times greater than MnO_2 nanozymes and a binding affinity 14.3 times higher than natural catalase. Complementing this, graphene-supported Cl–Cu–N_4-centered SANs (Cu–N_4ClG) were designed with atomic precision to replicate the coordination environment of natural SOD enzymes. These SANs not only catalyzed the dismutation of superoxide anions into oxygen and H_2O_2 but also displayed sequential CAT-like activity to decompose H_2O_2, thereby integrating dual catalytic pathways for ROS regulation. Their nitroxide radical scavenging and photothermally enhanced activity enabled effective protection of chondrocytes and alleviation of osteoarthritis.[83] More recently, cascade platforms have been explored to integrate complementary enzyme-like activities. A representative example is Pt@Cu–NC, a composite system in which CAT-like Pt nanoparticles are anchored onto Cu–N–C frameworks possessing intrinsic SOD-like activity. This architecture enabled a highly efficient ROS-scavenging cascade, with apparent rate constants 20-fold higher for superoxide anions and 390-fold higher for H_2O_2 elimination compared with mixed controls. Surface PEGylation enhanced dispersibility, stability, and biocompatibility, while cellular assays confirmed superior intracellular ROS removal.[84]

SANs-based optical and electrochemical techniques for environmental monitoring and remediation

Although SANs have become widely employed in biomedical applications, they have enormous untapped potential for use in environmental monitoring as well. Incorporating their unique catalytic and physicochemical properties into appropriately engineered optical or electrochemical platforms will play a vital role in realizing their full range of field applications.[25,26] In optical platforms, the SANs-catalyzed oxidation of chromogenic substrates can yield quantifiable colorimetric, fluorometric, or luminescence outputs, whereas in electrochemical platforms, SANs-driven redox events can be converted into measurable current or potential readouts. The following sections critically evaluate the latest advances in each technique, elucidate their operational strengths and inherent limitations, delineate their merits and limitations, and identify their specific advantages for pollutant detection and degradation applications.

Assay techniques

Colorimetric assays. Colorimetric-based SAN optical assays depend on a well-defined catalytic cycle in which the isolated metal centers (typically Fe, Co, Mn, or Ce coordinated as $M–N_x/S_x$ motifs) in SANs accelerate the one-

or two-electron reduction of H_2O_2 or dissolved O_2 to generate reactive oxygen species that oxidize chromogenic substrates such as TMB, OPD, or ABTS. The resulting quinone imine products exhibit strong visible absorption (*e.g.*, oxidized (ox) TMB at 652 nm), enabling direct optical transduction.[12,26,27] In contrast to metal/metal-oxide nanozymes, every metal atom in a SANs is catalytically accessible, lowering the activation barrier for substrate oxidation and pushing the detection limits into the nanomolar to picomolar range. For example, in colorimetric "turn-on" assays, the appearance of blue oxTMB ($\lambda \approx 652$ nm) or green oxABTS provides a direct optical indication of trace peroxides that are enzymatically or chemically generated by the target analyte. Conversely, SANs also enable "turn-off" colorimetric assays in which analytes bind to or block atomic active sites to suppress chromogenic turnover. For example, metallophilic interactions between Hg^{2+} or Ag^{+} and surface N/O ligands reduced the POD-like cycle of Ce–N–C SANs to realize selective visual detection of heavy metals.[27] Furthermore, the possibility of integrating dual enzyme-mimetic activities (*e.g.*, POD-like and OXD-like) within a single SAN broadens the potential of employing different substrates and facilitates the realization of ratiometric readouts that can help to mitigate common interference in complex environmental matrices. As a result, SANs-driven colorimetric assays can provide portable, low-cost, and highly sensitive tools for on-site environmental monitoring and pollutant remediation process tracking.

Fluorescence and ratiometric assays. Fluorescence-based SANs optical assays typically exploit the strong electron or energy transfer capabilities of atomically dispersed active centers to modulate the emissive state of a fluorogenic substrate. In the most common format, a single atom (*e.g.*, Fe, Ce, or Cu) catalyzes the selective redox conversion of a non-fluorescent precursor into a highly fluorescent product. The catalytic turnover frequency (or reaction kinetics) provides an optical signal with an intensity correlated to the concentration of the target analyte (*e.g.*, a peroxide, metal ion, or pesticide metabolite). An alternative mechanism relies on the SANs acting as an efficient fluorescence quencher through Förster resonance energy transfer, the inner filter effect, or photo-induced electron transfer. Binding of the analyte blocks or reverses this quenching, thereby regenerating the signal in a ratiometric fashion.[74] Because the catalytic sites are atomically isolated and all metal centers are maximally accessible, high turnover frequencies and detection limits that often reach the nanogram per milliliter level can be realized without the need for external oxidants. The absence of added peroxide is particularly advantageous in environmental matrices such as surface water or agricultural runoff, where residual disinfectants could otherwise generate false positives. Moreover, the optical nature of the result permits portable, chip-level, or smartphone-assisted analyses that facilitate rapid on-site screening of trace contaminants while retaining sufficient selectivity and quantitative accuracy for regulatory monitoring.

Electrochemical assays. Electrochemical assays for the detection of environmental pollutants generally operate by transducing redox events at an electrode–solution interface into electrical signals, namely steady-state currents in amperometry or peak currents/potentials in voltammetry. In a typical format, the target analyte (or a reporter species, such as H_2O_2, generated *in situ*) undergoes catalytic oxidation or reduction at the electrode surface; the magnitude, onset potential, or kinetic profile of this faradaic process constitutes the analytical result.[25] When SANs are immobilized on the electrode, each isolated metal center (*e.g.*, M–N_x, M–S_x, or dual-metal motif) functions as an atomically precise active site that can mediate the two-electron peroxide reduction, multi-electron oxygen reduction, or selective small-molecule oxidation with minimal overpotential. Because every metal atom is exposed and electronically coupled to a conductive scaffold, SANs deliver high turnover frequencies, enhance electron transfer kinetics, and suppress competing side reactions that would otherwise obscure the analytical signal.

These mechanisms provide several practical advantages for environmental monitoring. First, the reduced activation barriers and tailored redox potentials of SANs sites reduce operational voltages, thereby diminishing background currents and improving the limits of detection to the nanomolar or even picomolar level. Second, the chemical robustness of the surrounding carbon or oxide support endows SANs-modified electrodes with high tolerance to the wide pH ranges and dissolved-ion concentrations characteristic of natural and industrial water.[25] Third, the high dispersion of catalytically active atoms minimizes the use of precious metals while simultaneously mitigating fouling and prolonging sensor lifetimes during continuous deployment. Fourth, the nanoscale thickness and improved mechanical properties of SANs facilitate direct printing onto flexible substrates, enabling wearable devices that can stream real-time data. Moreover, SANs-functionalized amperometric and voltammetric assays can be readily coupled with electro-Fenton "sense-and-treat" configurations to realize simultaneous real-time monitoring and *in situ* remediation of environmental contaminants.[85]

SANs-assisted pollutant degradation and self-reporting systems

In addition to sensing, SANs-assisted "sense-and-destroy" platforms utilize atomically dispersed metal centers (*e.g.*, Fe–N_4, Co–N_4, and Cu–N_2) embedded in conductive carbon frameworks to realize dual-function active sites for both detection and degradation. For example, during the degradation stage, single-atom sites activate mild oxidants such as H_2O_2, peroxymonosulfate (PMS), or dissolved O_2 *via* Fenton- or Fenton-like one-electron pathways to produce highly reactive hydroxyl or sulfate radicals that non-selectively cleave chromophores, aromatic rings, and heteroatom bonds in dyes, antibiotics, and nitrosamines

even at near-neutral pH. In the self-reporting step, the same catalytic centers exhibit POD/OXD-like activity toward chromogenic probes (TMB, ABTS, and OPD) or electroactive reporters such that the instantaneous radical flux is translated into a proportional colorimetric, fluorometric, or amperometric signal. Essentially, SANs can deliver unified active sites where pollutant destruction ("kill") and reaction progress indication ("tell") are intrinsically coupled, enabling real-time on-site verification of remediation efficiency without external analytical instrumentation.

Applications of SANs in environmental analysis

Metal ion pollutants

Trace metal ions play critical roles as cofactors in numerous physiological processes; however, their excessive accumulation can lead to adverse effects ranging from neurotoxicity to carcinogenesis.[17] Industrial runoff, mining activities, and farm-chemical effluent have significantly polluted soils and aquatic systems with hazardous metal ions, especially Cr, Hg, As, Cd, and Pb.[17,27] Therefore, monitoring these toxic metal ions in environmental samples requires a rapid response, sub-nanomolar sensitivity, and low operational cost.[27] These requirements can be fulfilled by SANs-based sensors, as each isolated metal atom on the nanozyme surface functions as an active site, endowing the sensing platform with high selectivity and sensitivity.

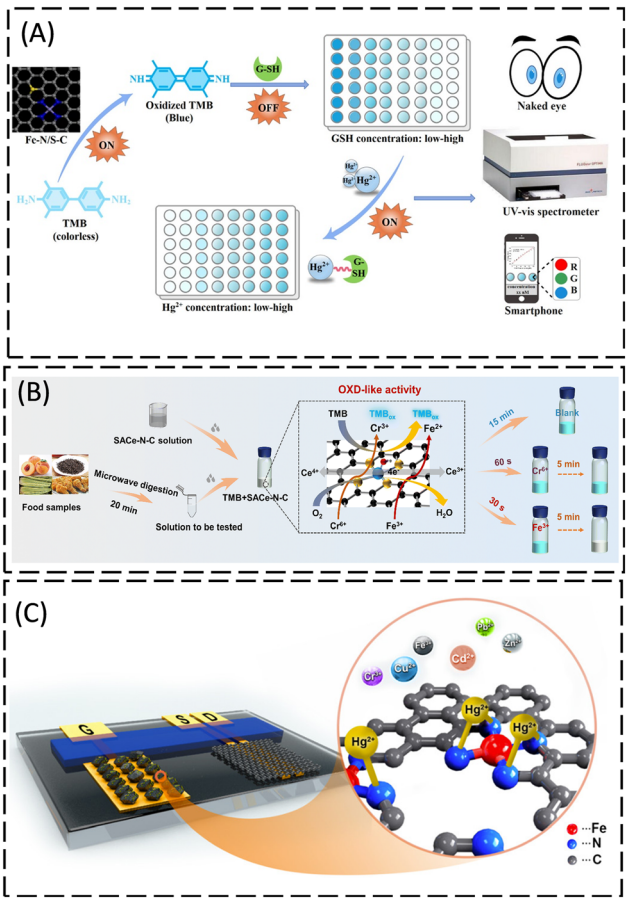

Fig. 3 (A) Fe–N/S–C SANs-based colorimetric sensor for ultrasensitive and multimodal mercury(II) ion detection, reproduced with permission from ref. 87, Copyright 2022, Elsevier B.V., (B) schematic illustration of the time-resolved Fe^{3+}/Cr^{6+} detection sensor utilizing the OXD-like activity of Ce–N–C SANs, reproduced with permission from ref. 89, Copyright 2015 RSC Publishing, and (C) real-time mercury ion sensing using a solution-gated graphene transistor functionalized with SANs, reproduced with permission from ref. 91, Copyright 2020 American Chemical Society.

Mao *et al.* immobilized isolated Fe atoms on single-layer N-doped graphene (SA-Fe/NG), reporting that chelation of 8-hydroxy-quinoline inhibited the POD-like oxidation of TMB, but competitive binding by Cr(VI) restored the blue oxTMB signal, yielding a linear detection range from 30 nM to 3 μM with a limit of detection (LOD) of 3 nM.[86] Compared with conventional nanozymes, the realization of 100% Fe utilization shortened the response time of SA-Fe/NG to below 2 min and enabled accurate determinations of Cr(VI) contents in tap- and fish-water extracts. Furthermore, Li *et al.* doped single Fe atoms into an N/S-coordinated carbon framework (Fe–N/S–C). In the presence of glutathione, the OXD-like pathway was blocked, and the subsequent addition of Hg^{2+} formed an Hg–S complex, releasing the catalytic sites and reviving the chromogenic reaction. A smartphone-assisted chip based on this "off/on" logic quantified Hg contents ranging from 1 nM to 10 μM with an LOD of 0.17 nM (Fig. 3A).[87]

Notably, single-atom Ce–N–C exhibited intrinsic phosphatase-like activity that was specifically inhibited by Al^{3+}; a ratiometric fluorimetric probe tracking the Ce^{3+}/Ce^{4+} cycle delivered an LOD of 22.98 ng mL^{-1} across 5–25 μg mL^{-1} accordingly, outperforming the drinking-water limit of 100 mg kg^{-1}.[88] Song *et al.* developed Ce–N–C SANs that exhibited OXD-like activity, reporting that Fe^{3+} and Cr^{6+} amplified the activity of Ce–N–C by accelerating Ce^{3+}/Ce^{4+} electron transfer. Based on this mechanism, they constructed a time-resolved sensor to detect Fe^{3+} and Cr^{6+} with LODs of 34.72 ng mL^{-1} (within 0.25–1.5 μg mL^{-1}) and 93.65 ng mL^{-1} (within 0.5–5 μg mL^{-1}), respectively, and recoveries of 88.66–113.24% and 85.49–111.22%, respectively. Additionally, the Ce–N–C OXD-like sensor enabled rapid quantification within 30 s (Fe^{3+}) and 60 s (Cr^{6+}) (Fig. 3B).[89] A recent study reported the synthesis of single-atom Ir-doped carbon dot nanozymes (Ir-CD SANs) *via in situ* pyrolysis. Maximizing the availability of Ir atoms enhanced the POD-like activity (178.81 U mg^{-1}) and aqueous stability (>30 d) of the Ir-CD SANs. This improvement enabled the sensitive colorimetric detection of Hg^{2+} within a linear range of 0.01–10 μM at an LOD of 4.4 nM.[90]

Although user-friendly, optical readouts may suffer from turbidity or background color interference; electrochemical transduction circumvents these issues and permits onsite microdevice integration. Yao *et al.* fabricated an Fe–N–C SANs functionalized solution-gated graphene transistor for detection of Hg^{2+}. The N atoms in the Fe–N–C SANs selectively chelate Hg^{2+}, while the catalytic site in SANs acts

as a signal amplifier. This design enables continuous tracking of Hg^{2+} with a LOD of 1 nM in drinking water, without requiring sample pre-treatment (Fig. 3C).[91] These early demonstrations suggest an approaching era of integrated SANs devices, including dip-in strips, catalytic paper, and 3D printed flow cells. Such devices can provide on-the-spot readouts and then self-neutralize toxic metal ions without causing secondary contamination. However, several key engineering challenges, such as preventing the agglomeration of isolated sites under radical attack, maintaining electron transport in thick catalytic layers, and designing macroporous supports to avoid pressure drops in continuous-flow reactors, remain to be addressed.

Organic pollutants

Organic pollutants, such as phenolic compounds, hydroquinone, and harmful gases, including volatile amines, formaldehyde, benzene, and toluene, are common products of industrial activities.[17] These compounds can react readily and build up in living organisms, posing serious threats to the environment and human health. Even at the sub-micromolar or sub-parts-per-million (ppm) levels, exposure to phenols induces oxidative stress in aquatic biota and compromise endocrine function in higher organisms, and the inhalation of volatile organics is linked to neurodegeneration and lung carcinogenesis.[17] Hydroquinone, a diphenolic isomer, has been widely used as a chemical precursor and synthetic intermediate in cosmetics, dyes, and pesticides. However, it is classified as a persistent organic pollutant in environmental systems owing to its high toxicity and poor biodegradability.[92] Therefore, the rapid detection of such organic pollutants in water and air could provide the data necessary to inform sound regulations and help deliver early alerts through environmental monitoring. Chu *et al.* converted an Fe-guanidine coordination lattice into nitrogen-doped graphene nanosheets hosting atomically dispersed Fe–N_4 sites (Fe-CNG).[92] The unique bidentate O/N coordination endowed each Fe center with an electron configuration favorable for the activation of dissolved O_2, producing both superoxide radicals and singlet oxygen under mildly acidic conditions. When applied in a TMB-based colorimetric assay, Fe-CNG converted a clear TMB solution into a blue product. This reaction was inhibited by the presence of hydroquinone or vitamin C, which caused the blue color to fade; thus, the extent of color change provided a direct measure of hydroquinone or vitamin C levels in the sample. The Fe-CNG SANs exhibited a linear response to hydroquinone in concentrations of 0.10–40 μM with an LOD of 0.025 μM and yielded quantitative recoveries of 96.7–104.3% for spiked hydroquinone in lake and tap water samples.[92]

Liu *et al.* developed hierarchically porous Fe/Mn–N–C diatomic nanozymes with a dodecahedral architecture by pyrolyzing Fe/Mn@ZIF-8 precursors capable of both sensitive optical detection and catalytic remediation in aqueous environments. The incorporation of Mn(II) acetylacetonate and ferrocene enriched the carbon matrix with Fe–N_x and Mn–N_x active centers, and the additional C–N functionalities increased the POD- and SOD-like activities. This catalytic property enabled highly selective and colorimetric detection of hydroquinone concentrations of 0–200 μM with an LOD of 0.216 μM. Together with H_2O_2, these nanozymes provided near-quantitative hydroquinone degradation and retained their efficiency over multiple reuse cycles (Fig. 4A).[93]

Lin *et al.* realized laccase-like reactivity using Fe_1@CN-20, a catalyst in which single Fe atoms are axially N-coordinated within a carbon matrix. In addition to successfully completing colorimetric assays, Fe_1@CN-20 detected and degraded a series of compounds, including 2,4-dichlorophenol, 4-chlorophenol, 2,6-dimethoxyphenol, catechol, phenol, and adrenaline (Fig. 4B). Indeed, this material quantified phenol concentrations as low as 2.6 μM within 0.0–50 μM and completely mineralized 2,6-dimethoxyphenol in ambient air, demonstrating the "detect-and-destroy" capability associated with many SANs.[94] More recently, Xia *et al.* dispersed Mn atoms on graphyne to create a colorimetric sensor array capable of discriminating five bisphenol analogs with LODs of 0.28–0.44 μM.[95] In parallel, Song *et al.* developed a portable dual-signal platform coupling Fe–N–C SANs with carbon quantum dots to monitor volatile amines generated during meat spoilage.[96] The atomically dispersed Fe–N_4 centers imparted a high POD-like activity (40.22 U mg^{-1}) that catalyzed the oxidation of colorless TMB to its blue form. In this platform, the oxidized TMB was strongly absorbed in the emission window of the carbon quantum dots, quenching their fluorescence through an inner filter effect. When volatile amines evolved from deteriorating meat, they chemically reduced the oxidized TMB back to its colorless form, thereby restoring the fluorescence of the carbon quantum dots while fading the blue color (Fig. 4C). This colorimetric–fluorescence dual-

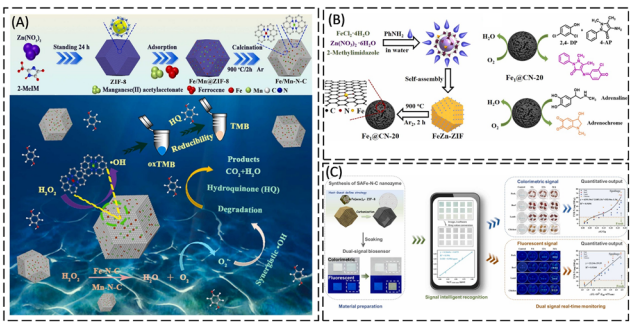

Fig. 4 (A) Synthetic route for Fe/Mn co-doped N–C SANs and integrated platform demonstrating hydroquinone quantification through colorimetric analysis coupled with oxidative degradation, reproduced with permission from ref. 93, Copyright 2023, Elsevier B.V., (B) preparation scheme for Fe_1@CN-20 SANs and their applications in simultaneous detection and degradation of 2,4-DP and adrenaline pollutants, reproduced with permission from ref. 94, Copyright 2022, Elsevier B.V., and (C) portable colorimetric–fluorescence dual-signal biosensor for visual detection of VA, reproduced with permission from ref. 96, Copyright 2023, Elsevier B.V.

Table 1 Summary of SANs-based detection/degradation platforms for metal ions and organic pollutants

Metal ions

S. No.	Material	Mechanism (enzyme mimic)	Signal output	Target	Linear range	Real sample	Limit of detection	Reference
1	Fe/NG SANs	POD-like	Colorimetric	Cr^{6+}	30 nM–3 μM	Tap water and tuna	3 nM	86
2	Fe–N/S–C SANs	POD-like	Colorimetric	Hg^{2+}	1 nM–10 μM	Tap water, lake water and seawater	0.17 nM	87
3	Ce–N–C SANs	Phosphatase-like	Fluorescence	Al^{3+}	5–25 μg mL^{-1}	Tofu, cake, and egg roll	22.89 ng mL^{-1}	88
4	Ce–N–C SANs	OXD-like	Colorimetric	Fe^{3+}/Cr^{6+}	0.25–1.5 μg mL^{-1} (Fe^{3+}) and 0.5–5 μg mL^{-1} (Cr^{6+})	Drinking water, tap water and wheat	34.72 ng mL^{-1} (Fe^{3+}) and 93.65 ng mL^{-1} (Cr^{6+})	89
5	Ir-CD SANs	POD-like	Colorimetric	Hg^{2+}	0.01–10 μm	Tap water, lake water and seawater	4.4 nM	90
6	Fe–N–C SANs	—	Transistor	Hg^{2+}	30 nM–3 μM	Drinking water	1 nM	91

Organic pollutants

S. No.	Material	Mechanism (enzyme mimic)	Signal output	Target	Linear range	Real sample	Limit of detection	Reference
1	Fe-SANs	OXD and laccase-like	Colorimetric	Hydroquinone	5–150 μM	Lake and tap water	0.025 μM	92
2	Fe–Mn–N SANs	POD- and SOD-like	Colorimetric and degradation	Hydroquinone	0–100 μM	—	0.216 μM	93
3	Fe_1@CN-20 SANs	Laccase-like	Colorimetric and degradation	Phenol	160–532 μM	—	2.6 μM	94
4	Graphyne-Mn SANs	POD-like	Colorimetric	Five bis-phenol analogues	1–1000 μM	Fruit cans	0.28–0.44 μM	95
5	Fe–N–C SANs	POD-like	Colorimetric/fluorescence	Volatile amine	0.5–50.0 ppm (colorimetric) and 0.5–50.0 ppm (fluorescence)	Livestock meat	0.98 and 0.083 ppm	96
6	Ru-SA/GF SANs	Laccase-like	Electrochemical	Hydroquinone, catechol, and resorcinol	0.1–80.1 μM; 80.1–380.1 μM (hydroquinone, catechol) and 0.1–800.1 μM (resorcinol)	Tap and river water	0.017, 0.023, and 0.038 μM	85

signal platform enabled the colorimetric detection of NH_3, exhibiting a linear trend within 0.5–50 ppm with an LOD of 0.984 ppm, as well as a fluorescence assay with an LOD of 0.0838 ppm.[96]

Wang *et al.* developed a photo-reduction method to synthesize single-atom Ru anchored on 3D porous graphene (Ru-SA/GF) that provided high metal exposure. Under identical conditions (2,4-dichlorophenol (2,4-DP), 50 mM, 50 μL; 4-aminoantipyrine (4-AP), 98 mM, 50 μL; PBS, 0.1 M, pH 6.8, 350 μL), Ru-SA/GF SANs exhibited biomimetic laccase-like activity comparable to natural laccase in catalytic mechanism, stability, and substrate specificity. The unique architecture of 3D porous graphene coupled with the maximally exposed Ru active sites enabled enhanced electrocatalytic oxidation of hydroquinone, catechol, and resorcinol, which correspond to distinct voltammetric peaks; this engineered Ru-SA/GF system achieved high simultaneous detection sensitivities for these three phenolic compounds with LODs of 0.017, 0.023, and 0.038 μM, respectively. Furthermore, the nanozymes exhibited excellent environmental remediation potential through efficient degradation of phenolic pollutants, establishing their dual functionality for sensing and wastewater treatment applications.[85] Table 1 lists the summary of SANs-based detection/degradation platforms for metal ions and organic pollutants.

Pesticides

Pesticide residues originating from intensive agriculture and agro-industrial runoff have become pervasive environmental contaminants. Many synthetic insecticides, herbicides, and fungicides possess high chemical stabilities, enabling them to persist in soil and water and bioaccumulate along the food chain.[2,17,26,97] Consequently, the rapid detection of pesticide residues in complex environmental samples is indispensable

for early warning surveillance. Wang *et al.* developed a colorimetric assay that combines SANs with a natural enzyme to quantify organophosphate pesticide (OP) residues. They produced Fe-based SANs (Fe–N/C) through one-step pyrolysis of alkaline lignin, yielding atomically dispersed Fe centers coordinated by pyrrolic N. These centers catalyze H_2O_2, generating hydroxyl radicals that oxidize TMB to its blue chromophore, thereby providing a measurable UV-visible light signal. Furthermore, the researchers included AChE in the system to impart pesticide selectivity, as it hydrolyzes acetylthiocholine (ATCh) to thiocholine (TCh), which suppresses the TMB color change. This detection mechanism relies on the chlorpyrifos-mediated inhibition of AChE, which enabled the Fe–N/C nanozyme to restore TMB oxidation, resulting in a measurable change in absorbance. When quantified through these absorbance variations, the chlorpyrifos concentration demonstrated a linear response within 0.05–10.0 μg mL^{-1} at an LOD of 2.11 ng mL^{-1}.[98]

In another study, researchers developed an Fe–N–C catalyst by combining isolated Fe atoms with small Fe clusters on N-doped porous carbon (FeAC/FeSA-NC) obtained by pyrolyzing an Fe(II)–phenanthroline complex embedded in a ZIF-8 template to guide uniform metal dispersion. The resulting nanozymes exhibited strong OXD-like activity, converting dissolved oxygen into superoxide radicals. A high catalytic rate was observed for these SANs; DFT calculations indicated that this occurred because neighboring single atoms and clusters lowered the reaction energy barrier. Therefore, the researchers applied the FeAC/FeSA-NC SANs as a ratiometric fluorescent probe to detect AChE activity and OPs. Notably, the thiol products of AChE inhibited these SANs, whereas OPs blocked AChE and restored the signal. The resulting assay exhibited a linear response from 0.005 to 50 ng mL^{-1} with an LOD of 1.9 pg mL^{-1}.[99]

Lyu *et al.* developed Fe-based SANs for herbicide detection by carbonizing hemin inside a ZIF-8 framework. The isolated Fe–N sites mimicked the active centers of natural peroxidase and endowed the material with strong POD-like activity. The researchers developed a point-of-care test for a target herbicide, 2,4-dichlorophenoxyacetic acid (2,4-D), using Fe-SANs as a label in a lateral flow immunoassay strip. The strip exhibited a linear response from 1 to 250 ng mL^{-1} with an LOD of 0.82 ng mL^{-1}. It also discriminated between 2,4-D and similar phenoxy herbicides. Tests on human urine confirmed that the device can quickly and accurately measure 2,4-D exposure, highlighting its promise for the portable and sensitive monitoring of herbicide contamination (Fig. 5A).[100]

Other researchers devised a dual-mode, broad-spectrum aptamer sensor combining colorimetric and electrochemical transduction to monitor OPs in vegetable matrices. The core catalyst comprised a single-atom Fe nanozyme (SA-Fe-NZ) obtained by carbonizing Fe-doped ZIF-8. The atomically dispersed Fe centers in the SANs exhibited robust POD-like activity that oxidized colorless TMB to its blue product. Upon binding to its OP target, the aptamer–OP complex

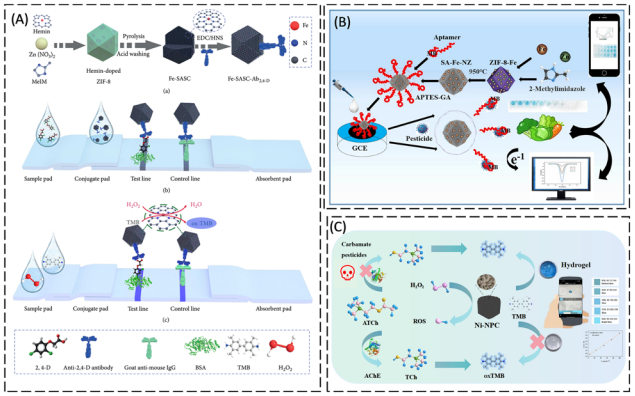

Fig. 5 (A) Schematics showing Fe-SASC synthesis, antibody conjugation (Fe-SASC-$Ab_{2,4\text{-}D}$) and the Fe-SASC-based lateral-flow immunoassay strip for 2,4-D detection, reproduced with permission from ref. 100, Copyright 2022, AAAS, (B) a scheme showing the assembly and detection process of the SA-Fe SANs dual-mode biosensor, reproduced with permission from ref. 101, Copyright 2024, Elsevier B.V, and (C) Ni–NPC SANs platform for carbamate pesticide remediation and smartphone visualization, reproduced with permission from ref. 103, Copyright 2024, American Chemical Society.

inhibited the SA-Fe-NZ, suppressing catalytic turnover and producing an OP concentration-dependent decrease in the colorimetric signal. Simultaneously, the SA-Fe-NZ amplified the electrochemical signal, enabling a parallel voltammetric readout (Fig. 5B). This integrated sensor exhibited a wide dynamic range (10^{-13}–10^{-2} M), an extremely low LOD of 3.55 fM, and high selectivity and satisfactory recoveries in real vegetable samples.[101]

Furthermore, a recent study developed a smartphone-assisted colorimetric paper sensor for the on-site determination of carbofuran (CBF) residues by harnessing the high POD-like activity of Ni–N–C SANs synthesized from $Ni(OH)_2$ nanoplates. The sensing mechanism relied upon the hydrolysis of ATCh to TCh by AChE, which in turn suppressed the nanozyme-catalyzed oxidation of colorless TMB to blue oxTMB. The presence of CBF inhibited AChE activity, decreasing TCh production. This, in turn, restored the Ni–N–C catalytic cycle, yielding a concentration-dependent blue color that could be quantitatively evaluated using a smartphone camera. The paper sensor exhibited a linear response from 10 to 500 ng mL^{-1} with an LOD of 8.79 ng mL^{-1} and demonstrated recovery rates of 81.1–125.3% when applied to Chinese cabbage, conventional cabbage, and lettuce.[102]

Electrochemical sensors employing SANs have also been developed for pesticide detection and remediation. Xu *et al.* dispersed single Ni atoms within a nitrogen-doped porous-carbon matrix (Ni–NPC) to create uniformly accessible Ni–N_4 catalytic sites. Under a mild potential window, this nanozyme-catalyzed peroxymonosulfate (PMS) activation generated sulfate and hydroxyl radicals that rapidly oxidized the carbamate pesticide carbaryl (Fig. 5C). Chronoamperometry indicated an anodic current increase of ~200 μA cm^{-2}, reflecting the *in situ* electro-oxidative

Table 2 Summary of SANs-based detection assays for pesticides

Pesticides								
S. No.	Material	Mechanism (enzyme mimic)	Signal output	Target	Linear range	Real sample	Limit of detection	Reference
1	Fe–N/C SANs	POD-like	Colorimetric	Chlorpyrifos	0.05–10.0 μg mL^{-1}	Soil samples	2.11 ng mL^{-1}	98
2	Fe–N–C SANs	OXD-like	Fluorescence	Organophosphorus pesticides	0.005–50 ng mL^{-1}	Tap water	1.9 pg mL^{-1}	99
3	Fe-SAC	POD-like	Lateral flow assay	2,4-Dichlorophenoxyacetic acid	1–250 ng mL^{-1}	Real human urine samples	0.82 ng mL^{-1}	100
4	Fe-SANs	POD-like	Colorimetric and electrochemical	Organophosphorus pesticides	10^{-13}–10^{-2} M	Vegetable samples	7.54 and 3.55 fM	101
5	Ni–N–C SANs	POD-like	Colorimetric	Carbofuran	10–500 ng mL^{-1}	Vegetable samples	8.79 ng mL^{-1}	102
6	Ni–NPC SANs	POD-like	Colorimetric	Carbamate	5–100 ng mL^{-1}	Lake water and pakchoi	1.5 ng mL^{-1}	103

conversion of the analyte, and high-performance liquid chromatography confirmed 90% degradation within 60 min. Furthermore, observing the electrode with a smartphone camera allowed real-time RGB evaluation of colorimetric indicators, enabling on-site quantification without requiring laboratory infrastructure. This integrated "sense-and-destroy" strategy enables ultrasensitive electrochemical detection with simultaneous catalytic remediation in portable pesticide-monitoring platforms.[103] Table 2 gives the summary of SANs-based detection assays for pesticides.

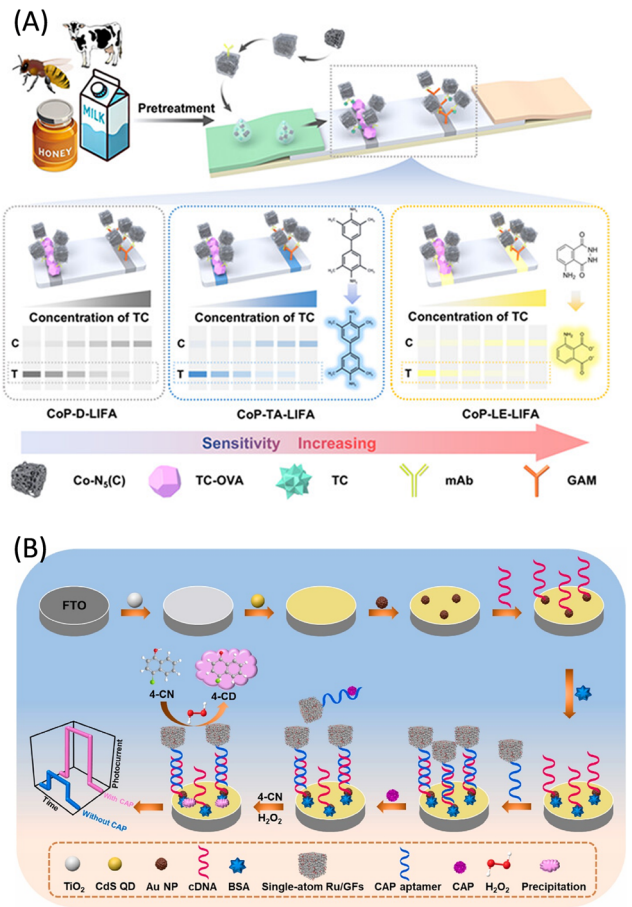

Fig. 6 (A) Schematic illustration showing the cobalt SANs-enhanced multimodal lateral flow immunoassay for on-site tetracycline detection, reproduced with permission from ref. 105, Copyright 2025, American Chemical Society and (B) schematic diagram showing the Ru SANs-enhanced PEC aptasensor for ultrasensitive CAP detection, reproduced with permission from ref. 106, Copyright 2025, Elsevier B.V.

Drug residues

The widespread use of antibiotics and other medicines has resulted in the entry of these drug residues into water, soil, and food chains worldwide.[97] Many of these compounds and their deterioration products readily gain or lose electrons, making them excellent targets for redox-based detection. As a result, SANs with POD-, OXD-, or SOD-like catalytic properties are now widely used to sense antibiotic pollutants and break them down in real time.

For example, researchers developed SANs by anchoring isolated Pt atoms onto carbon nitride nanorods (SA-Pt/g-C_3N_4–K) to realize the colorimetric detection of oxytetracycline (OTC). In this colorimetric assay, the POD-like Pt═O sites on SA-Pt/g-C_3N_4–K generated hydroxyl radicals that oxidized colorless TMB to blue oxTMB. By using an OTC-specific DNA aptamer to temporarily block the catalytic pocket, color appeared only when OTC displaced the aptamer (a "turn-on" effect). This assay exhibited a linear response from 0.06 to 0.90 mg L^{-1} for OTC with an LOD of 10.3 μg L^{-1}. In addition, the SANs-mediated radical production resulted in strong antibacterial activity.[104]

Furthermore, researchers have fabricated Co-based SANs *via* template-assisted pyrolysis to realize atomically dispersed Co centers in a Co–N_5 coordination environment. Steady-state kinetics revealed pronounced POD-like behavior, and the catalyst generated substantial quantities of reactive oxygen species that amplified both colorimetric and chemiluminescence signals. Using these unique properties, Huang *et al.* developed a multimodal lateral-flow immunoassay for tetracycline (TC) that combined naked-eye color detection, catalytic signal enhancement, and quantitative chemiluminescence data to achieve LODs of 0.091, 0.062, and 0.056 ng mL^{-1} for the three detection modes (Fig. 6A).[105]

Table 3 List of SANs-based detection/degradation platforms for drug residues and organic dyes

Drug residues

S. No.	Material	Mechanism (enzyme mimic)	Signal output	Target	Linear range	Real sample	Limit of detection	Reference
1	Pt/g-C_3N_4–K SANs	POD-like	Colorimetric	Oxytetracycline	60–900 μg L^{-1}	—	10.3 μg L^{-1}	104
2	Co-SANs	POD-like	Lateral flow assay	Tetracycline	0.1–25 ng mL^{-1}	Milk and honey samples	0.091 ng mL^{-1}	105
3	Ru/GF SANs	POD-like	Photoelectrochemical	Chloramphenicol	0.01–50 nM	River and honey samples	4.12 pM	106
4	Fe/Cu dual-SANs	POD-like	Colorimetric detection and degradation	Isoniazid detection and levofloxacin degradation	0.9–10 μM	Urine (isoniazid) and simulated pollutant (levofloxacin)	0.3 μM	107

Dyes

S. No.	Material	Mechanism (enzyme mimic)	Signal output	Target	Linear range	Real sample	Limit of detection	Reference
1	ZnBNC SANs	POD-like	Colorimetric	*p*-Phenylenediamine	0.3–10 μM	Hair dyes and dyed hair samples	0.1 μM	109
2	Mn-SANs	POD-like	Degradation	Methylene blue	—	Tap water and lake water	—	110
3	Fe–NC SANs	POD and laccase-like	Degradation	Rhodamine B	—	Simulated complex water samples	—	111
4	Fe/Bi dual-SANs	OXD-like	Degradation	Rhodamine B	—	—	—	112
5	Fe–N–C SANs	OXD, POD-, and CAT-like	Degradation	Rhodamine B	—	—	—	113

In another study, researchers developed a SANs-based photoelectrochemical aptasensor in which atomically dispersed Ru centers catalyzed a precipitation reaction that amplified the signal, enabling ultra-trace detection of chloramphenicol (CAP). The atomically dispersed Ru centers exhibited exceptional POD-like activity, rapidly oxidizing 4-chloro-1-naphthol (4-CN) to form an insulating precipitate on the electrode surface that markedly suppressed the photocurrent. The introduction of CAP liberated the surface-bound aptamer through high-affinity binding, preventing 4-CN deposition, restoring the photocurrent, and thereby generating a sensitive "signal-on" response. Moreover, when coupled with a high-efficiency photoactive trilayer comprising Au nanoparticles, CdS quantum dots, and TiO_2, the self-powered photoelectrochemical aptasensor achieved an LOD of 4.12 pM for CAP with excellent selectivity and analytical accuracy (Fig. 6B).[106]

Xie *et al.* developed a 3D hollow porous nano-architecture (Fe/Cu–NC) hosting atomically dispersed Fe–N_x and Cu–N_x sites using a salt-templated freeze-drying/pyrolysis process. The synergistic effects of the dual single-atom centers enhanced the POD-like activity of Fe/Cu–NC, leading the researchers to apply it in a chromogenic assay for isoniazid (INH) detection. In the presence of H_2O_2, this nanozyme oxidized colorless TMB to its blue-oxidized form, and the presence of INH subsequently reduced the chromophore, producing a concentration-dependent bleaching effect. The developed sensor exhibited a linear response to INH over 0.9–10 μM with an LOD of 0.3 μM.[107] In addition to sensing, the same Fe/Cu dual active sites efficiently activated PMS to generate reactive oxygen species that mineralized 90.4% of 10 mg L^{-1} levofloxacin within 30 min under optimal conditions, confirming its practicality as a "detect-and-destroy" platform.[107] This research underscores how hetero-bimetallic single-atom coordination not only enhances catalytic turnover but also broadens the substrate scope to provide a versatile platform for simultaneous antibiotic monitoring and remediation. Table 3

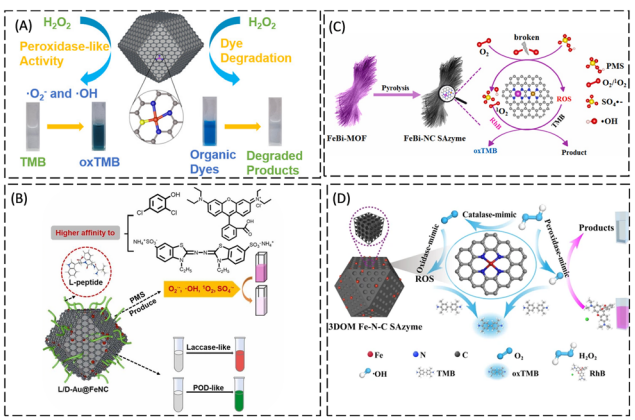

Fig. 7 (A) Scheme depicting enhanced peroxidase-mimicking activity in Mn-based SANs for catalytic dye decomposition, reproduced with permission from ref. 110, Copyright 2023, American Chemical Society, (B) schematic illustration of chiral Fe–N–C single-atom nanozymes exhibiting multi-enzyme activity for organic dye degradation, reproduced with permission from ref. 111, Copyright 2024, Elsevier B.V., (C) scheme depicting Fe/Bi dual SANs enabling cascade catalysis and PMS activation for efficient dye degradation, reproduced with permission from ref. 112, Copyright 2022, Elsevier B.V., and (D) atomically dispersed Fe–N–C single-atom nanozymes with hierarchical porosity for RhB dye degradation, reproduced with permission from ref. 113, Copyright 2025, Elsevier B.V.

summarizes various SANs-based detection/degradation platforms for drug residues.

Organic dyes

Synthetic organic dyes, such as methylene blue (MB), rhodamine B (RhB), methyl orange, p-phenylenediamine (PPD), and crystal violet, are widely used in the textile, printing, and cosmetic industries.[17,108] However, these compounds exhibit high chemical stabilities and slow degradation processes, and their toxicity poses significant risks to aquatic ecosystems and human health even at low concentrations.[17] Over the past five years, SANs-based frameworks have been widely used in the detection and degradation of such dyes.

For example, Feng *et al.* reported the controllable synthesis of B-doped Zn–N–C (ZnBNC) SANs exhibiting strong POD-like activity. Exploiting this activity, they established a colorimetric assay for PPD that provided high sensitivity and selectivity with a broad linear response range of 0.3–10 μM and a low LOD of 0.1 μM, suggesting its suitability as an alternative analytical approach for identifying PPD in commercial hair dye formulations and dyed hair samples.[109] In another study, Feng *et al.* stabilized isolated Mn atoms within a triple N–, P–, and S-doped carbon scaffold (Mn-SANs) using a sacrificial-template strategy.[110] Experiments confirmed that Mn doping significantly enhanced catalytic activity, and the Mn-SANs efficiently degraded organic dyes to achieve 90% MB removal within 300 min, even with minimal nanozyme loading across broad pH ranges. Free radical quenching experiments and EPR analysis revealed that superoxide and hydroxyl radicals played crucial roles in the degradation mechanism (Fig. 7A).[110]

Furthermore, Ning *et al.* synthesized chiral Fe–N–C SANs by incorporating chiral tripeptides (L/D-Pen–Phe–Trp) exhibiting laccase-like and POD-like activities for PMS activation and catalytic dye degradation. Molecular docking showed that the different activities of the L- and D-configured materials arose from the different binding affinities between the chiral peptide environments and target substrates. Further modification with Au produced chiral L-/D-Au@FeNC SANs that exhibited even higher catalytic and dye degradation performance owing to the improved dispersion stability in water imparted by the chiral peptides. Computational analysis indicated that the L-peptide bound more strongly to RhB, ABTS, and 2,4-dichlorophenol than the D-peptide. Consistent with this result, the L-Au@FeNC exhibited stronger enzyme-like activity than its D-counterpart and activated PMS more effectively to degrade RhB. Indeed, the L-Au@FeNC/PMS system rapidly and efficiently decomposed RhB by generating multiple reactive species (superoxide, hydroxyl, singlet oxygen, and sulfate radicals) while maintaining catalytic stability over repeated degradation cycles (Fig. 7B).[111]

In another study, Chen *et al.* developed bimetallic SANs (FeBi–NC) derived from an Fe-doped Bi-MOF precursor. These SANs feature co-existing Fe–N_4 and Bi–N_4 dual active sites on a carbon support for AChE detection and dye degradation applications. The results of X-ray absorption near-edge structure and EXAFS analyses confirmed the atomic dispersions of both metal sites with high loadings of Fe (2.61 wt%) and Bi (8.01 wt%). The Fe/Bi–NC SANs exhibited remarkable OXD-like activity, exceeding those of Fe–NC and Bi–NC by 5.9 and 9.8 times, respectively. When coupled with AChE, the Fe/Bi–NC formed a cascade enzyme–nanozyme system that achieved ultrasensitive AChE detection with a low LOD of 1×10^{-4} mU mL^{-1}. The synergistic Fe–N_4 and Bi–N_4 sites exhibited strong PMS activation capabilities facilitated by enhanced electron transfer, generating reactive intermediates for rapid RhB dye degradation. By exploiting this dual-site catalysis, Fe/Bi–NC achieved 100% RhB removal within 5 min *via* PMS activation, demonstrating excellent efficiency in pollutant degradation (Fig. 7C).[112]

Wu *et al.* used Fe–N–C SANs featuring atomically dispersed Fe–N_4 sites on a 3D hierarchically ordered microporous–mesoporous–macroporous N-doped carbon matrix (3DOM Fe–N–C) for efficient RhB degradation. The 3D porous architecture enhanced mass transfer and active site accessibility, while the high metal utilization conferred superior triple-enzyme-mimicking activities (OXD-, POD-, and CAT-like). Relying on the POD-like activity, 3DOM Fe–N–C effectively degraded RhB *via* hydroxyl radicals generated from H_2O_2 (Fig. 7D).[113] Table 3 lists the summary of SANs-based detection/degradation platforms for organic dyes.

Microbial hazards

Microbial contaminants, including pathogenic bacteria, fungi, viruses, and their toxins, have escalated into a critical public health burden that accounts for an estimated seven million deaths annually.[114] This increasing burden is largely attributed to the emergence of new antibiotic-resistant pathogenic strains. Notably, the atomic utilization and uniformity of active sites allow SANs to generate controllable bactericidal reactive oxygen/nitrogen species (ROS/RNS). Moreover, the tunable coordination environments of SANs permit switching between POD-, OXD-, Fenton-, CAT-, and haloperoxidase-like as well as Fenton and nitric-oxide releasing pathways, enabling broad-spectrum microbial inactivation while reducing reliance on conventional antibiotics.

For example, Dai *et al.* developed SANs comprising Cu atoms anchored on atomically thin carbon nitride nanodots (Cu–CNNDs) for use as an antibacterial textile coating. These nanozymes exhibited a high POD-like catalytic efficiency (up to 8.09×10^5 M^{-1} s^{-1}) comparable to that of natural enzymes. The results of experimental and theoretical analyses revealed that this catalytic activity arose from the nanoscale size effect of the C_3–N_4 support, which optimized the coordination environment of the single Cu atoms. This structural refinement ensured the complete exposure of the Cu–N_3 active sites, significantly enhancing the activation of H_2O_2 to

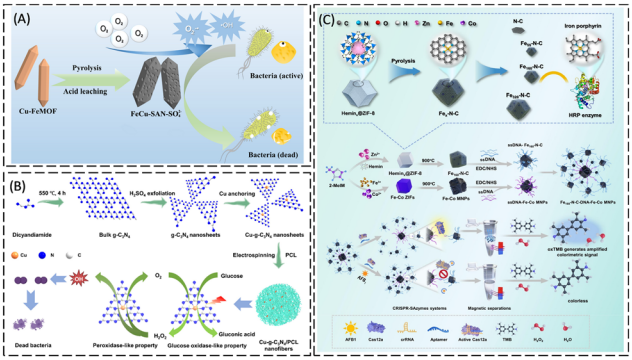

Fig. 8 (A) Schematic representation of the antibacterial mechanism in the Fe–Cu SANs system, reproduced with permission from ref. 116, Copyright 2025, American Chemical Society, (B) synthesis of Cu–g-C_3N_4/PCL nanofibers and the light-dependent dual-enzyme mimicking mechanism for antibacterial applications, reproduced with permission from ref. 117, Copyright 2025, American Chemical Society, and (C) schematics of Fe–N–C SANs synthesis, Fe–N–C/Fe–Co MNP fabrication and CRISPR-SANs biosensor operation, reproduced with permission from ref. 120, Copyright 2024, Elsevier B.V.

generate hydroxyl radicals. Notably, the Cu–CNNDs demonstrated considerable antibacterial efficacy, achieving >99% bacterial inactivation. Critically, their successful integration into cotton fabrics highlights their potential for practical applications in antimicrobial textiles.[115]

A recent study synthesized sulfate-modified Fe–Cu bimetallic SANs (FeCu-SANs-SO_4^{2-}) using high-temperature pyrolysis and sulfation of an eco-friendly Cu–Fe MOF precursor. The as-prepared FeCu-SANs-SO_4^{2-} demonstrated suitable OXD-like catalytic activity that was attributed to the synergistic interaction among the Fe–Cu dual active sites, a high specific surface area of 202 m^2 g^{-1}, and a well-defined mesoporous structure with an average pore size of 11.08 nm. Notably, the incorporation of Brønsted acidic sites enabled the nanozymes to overcome pH-dependent activity limitations while exhibiting superior thermal and long-term storage stabilities compared with those of natural enzymes. At a concentration of 0.1 mg mL^{-1}, FeCu-SANs-SO_4^{2-} achieved a bactericidal efficiency exceeding 90% against *Escherichia coli*, *Staphylococcus aureus*, *Aeromonas hydrophila*, and *Edwardsiella tarda* without requiring external stimuli. This excellent antibacterial performance was primarily attributed to the ability of the SANs to generate ROS efficiently, particularly superoxide anions and hydroxyl radicals. This induced oxidative stress by extracting electrons from essential bacterial cellular components, leading to irreversible damage (Fig. 8A).[116]

Wu *et al.* developed SANs using Cu anchored to graphitic carbon nitride nanosheets (Cu–g-C_3N_4) which exhibited OXD- and POD-like properties, enabling cascade catalytic reactions for ROS generation. The as-prepared bifunctional nanozymes exhibited broad-spectrum antibacterial efficacy against both Gram-positive and Gram-negative multidrug-resistant bacterial strains. Under visible light irradiation, Cu–g-C_3N_4 exhibited GOx-like activity, catalyzing glucose oxidation to produce H_2O_2, whereas in the dark, it functioned as a POD-like nanozyme, decomposing H_2O_2 into highly reactive hydroxyl radicals. This self-sustaining cascade reaction ensured continuous ROS generation, leading to potent antibacterial effects. Notably, Cu–g-C_3N_4 outperformed pristine g-C_3N_4 and other metal-modified variants (*e.g.*, Cr–, K–, Fe–, and Zn–g-C_3N_4) owing to its enhanced light absorption and optimized surface adsorption properties. Researchers incorporated Cu–g-C_3N_4 into polycaprolactone (PCL) nanofibers *via* electrospinning to obtain Cu–g-C_3N_4/PCL nanofiber dressings for infected wound management. These dressings effectively eradicated bacterial infections and accelerated tissue regeneration in murine skin wound models (Fig. 8B).[117]

In addition to pathogenic microorganisms, toxic metabolic by-products, such as mycotoxins, are significant environmental pollutants that threaten ecological and human health. Therefore, SANs-based detection strategies have been developed for these substances as well. For example, Shen *et al.* engineered Fe-based SANs with an optimized Fe–N_3PS active moiety embedded in N-, P-, and S-co-doped hollow carbon nanocages (Fe–N_3PS/HC). The results of DFT calculations indicated that co-doping with P and S effectively modulated the electronic environment of the Fe center in these SANs, lowering the reaction barriers and thereby boosting their POD-like activity both kinetically and thermodynamically. This enhanced reactivity realized a three-channel nanozyme sensor array coupling Fe–N_3PS/HC with orthogonal chromogenic reactions. The resulting platform yielded analyte-specific color signatures that enabled rapid visual discrimination of five toxins: aflatoxin B1 (AFB_1), aflatoxin B2, zearalenone (ZEN), fumonisin B2 (FB_2), and deoxynivalenol (DON). A multivariate statistical analysis indicated that this array reliably differentiated these five mycotoxins as well as ten metal ions at trace levels (ng mL^{-1} and low μM, respectively).[118]

In another study, Zhang *et al.* synthesized Co- and Fe-based SANs (M/N-PC, where M denotes Co or Fe) to evaluate their efficacy in mycotoxin degradation. The Co/N-PC SANs featured Co–N_4 sites alongside Co nanoclusters and achieved 99.4% patulin degradation within 60 min, outperforming Fe/N-PC (with Fe–N_5 sites alone); a DFT analysis attributed this enhancement to the synergistic effect between the Co–N_4 sites and nanoclusters, which elevated the electron density near the Fermi level, boosting catalytic activity. The degraded by-products exhibited negligible cytotoxicity, and M/N-PC demonstrated broad pH adaptability and reusability, confirming its utility for mycotoxin removal from food products (*e.g.*, apple juice). Notably, the M/N-PC system also efficiently degraded AFB_1, DON, and ZEN by nearly 100% within 10–40 min, confirming its versatility in food safety applications.[119]

In a complementary approach, Liu *et al.* synthesized Fe_{160}–N–C SANs and Fe–Co magnetic nanoparticles (MNPs) *via* pyrolysis. The Fe_{160}–N–C SANs exhibited high POD-like activity and were employed as TMB chromogenic catalysts in

a CRISPR/Cas12a-based colorimetric aptasensor for AFB_1 detection accordingly. In the absence of AFB_1, the aptamer bound to CRISPR RNA, activating the trans-cleavage activity of Cas12a, which released Fe_{160}–N–C SANs into the supernatant and oxidized TMB into a blue product. However, when AFB_1 was added, aptamer–target binding inhibited Cas12a activation, reducing the signal output. Critically, this study introduced an innovative CRISPR/Cas-based biosensor that integrates Fe_{160}–N–C SANs and MNPs, eliminating the need for target pre-amplification while enabling room-temperature detection. This system achieved a sensitivity of 1.5×10^{-7} ng μL^{-1} over a broad linear range (10^{-6}–1 ng μL^{-1}), surpassing the performance of conventional AFB_1 detection methods (Fig. 8C).[120]

Conclusions, limitations and future prospects

The dispersion of individual metal atoms on heteroatom-doped supports in SANs maximizes active component utilization, making them ideal catalytic platforms for environmental monitoring and remediation. Although SANs showed promise, they still lack the ability to mimic the complex microenvironments that are responsible for the catalytic precision seen in natural enzymes. For example, SANs typically mimic only the primary coordination shell, usually a metal atom coordinated with nitrogen, phosphorus, or sulfur atoms, while lacking the flexible structural dynamics and allosteric regulatory features that natural enzymes use to modulate activity. Moreover, natural enzymes operate within uniquely tailored environments that feature specific hydrophobic/hydrophilic regions, local pH gradients, and detailed electrostatic interactions, all of which are difficult to reproduce using current SAN designs. These characteristics are important not only for achieving high substrate specificity but also for reducing unwanted side reactions and improving catalytic efficiency.[6,10] This fundamental limitation in mimicking enzyme-like environments restricts the broader use of SANs in reactions that demand high selectivity or function in complex biological settings. Additionally, challenges persist in scaling up atomically precise synthesis and ensuring long-term biocompatibility. While SANs offer greater precision and catalytic performance than conventional nanozymes, their design still lacks the self-regulating behavior and adaptive catalysis intrinsic to biological enzymes. Addressing this challenge will require progress in multi-shell coordination design, the use of advanced supramolecular frameworks, or the integration of protein–inorganic hybrid systems that more closely resemble the functional environments of natural enzymes.

Additionally, the precise structure–function correlations of SANs remain unclear for many systems. Although advanced characterization techniques (*e.g.*, aberration-corrected TEM and synchrotron X-ray absorption spectroscopy) reveal coordination environments in SANs, significant challenges persist in resolving site heterogeneity and monitoring of dynamic structural evolution during catalytic reactions. Furthermore, present synthetic approaches of SANs face significant limitations, as conventional high-temperature pyrolysis and complex templating methods typically restrict metal loading to <2 wt%, while introducing batch-to-batch inconsistencies. Moreover, high-temperature processing induces structural degradation, including carbon framework collapse and bond cleavage, thereby undermining the long-term stability of M–N–C frameworks. Besides, significant challenges arise when transitioning SANs from controlled laboratory conditions to real-world applications. For example, complex environmental matrices including humic acid-rich river water, high-salinity industrial effluents, and colloidal soil extracts can deactivate catalytic sites or scavenge reactive oxygen species, substantially reducing performance. As a result, though promising "sense-and-destroy" concepts have been demonstrated, the development of fully integrated systems capable of real time detection and pollutant degradation remains limited.

To overcome current limitations, interdisciplinary approaches that make use of computational methods like DFT will be indispensable for advancing the rational design of SANs. For instance, DFT can provide atomistic insights into the electronic structure of metal centers, enabling prediction of how coordination environments influence reactivity. For advanced oxidation processes, DFT can be used to simulate the adsorption energies of oxidants (*e.g.*, H_2O_2 and PMS) and pollutants, map charge transfer pathways, and evaluate energy barriers for ROS generation. These predictive capabilities will help design SANs with high activity and stability under the harsh oxidative conditions typical of environmental remediation. Emerging low-temperature synthesis methods, such as plasma-enhanced chemical vapor deposition (CVD) and metal–organic CVD, may enable higher single-atom loadings while maintaining structural integrity.[121] Enhancing metal–support interactions through defect-engineered carbon or covalent organic frameworks could prevent active site aggregation.[122,123]

The synergistic integration of multiple enzyme-like activities represents an important strategy to enhance the catalytic efficiency and functional versatility of SANs. Although conventional nanozymes are typically restricted to demonstrating one dominant catalytic function, for SANs, owing to their structurally tunable active centers, unique opportunities are provided for designing dual-, tri-, and multi-enzyme systems. For example, Fe–N_4 SANs have been reported to exhibit both POD- and CAT-like activities, enabling the scavenging of ROS during oxidative stress in cells.[56] Moreover, coupling SANs with natural enzymes represents a promising strategy to construct cascade enzyme–nanozyme systems, thereby enhancing target specificity and achieving high selectivity.[112] These multi-enzyme activities are valuable for cascade reactions, allowing applications in pollutant degradation, synergistic antibacterial therapies, and sensitive biosensing. Moreover, dual-active-site designs (*e.g.*,

Fe/Bi pairs) can also be used for cascade degradation processes in environmental applications. Future work must elucidate the atomic-scale mechanism of this multi-enzyme cooperation and develop generalizable synthetic strategies to reliably achieve these multifunctional properties.

For practical applications, materials must be engineered to resist environmental fouling while maintaining catalytic accessibility. Surface modifications with tailored hydrophilicity and hierarchically porous architectures, such as Fe/Mn–N–C sponges with microfluidic channels, could address this challenge. Comprehensive toxicity assessments are needed to evaluate metal leaching and reactive by-products throughout the material lifecycle. Incorporating SANs into functional materials like membranes or 3D-printed cartridges could enable continuous monitoring and treatment. Expanding target pollutants beyond conventional models to include emerging contaminants like pharmaceuticals and microplastic additives will require precise control over reactive species generation. Selective oxidation pathways must be engineered through coordination environment tuning to avoid nonspecific reactions. As highlighted by recent studies, scaling up SANs production with environmentally benign methods and establishing standardized performance metrics will be essential for real-world implementation. Through coordinated efforts in computational design, materials engineering, and environmental safety assessment, SANs can evolve from laboratory level prototypes into practical solutions for next-generation environmental monitoring and remediation. Their unique combination of atomic precision and robust performance positions them as transformative tools for addressing complex pollution challenges.

Author contributions

Arumugam Selva Sharma: conceptualization, writing – original draft, writing – review and editing, visualization. Nae Yoon Lee: writing – review and editing, supervision, funding acquisition.

Conflicts of interest

There are no conflicts to declare.

Data availability

No primary research results, software, or code have been included and no new data were generated or analyzed as part of this review.

Acknowledgements

This research was supported by the National Research Foundation of Korea (NRF) grant funded by the Korea government (MSIT) (RS-2023-00208684) and also by the Basic Science Research Program through the National Research Foundation of Korea (NRF) funded by the Ministry of Education (RS-2021-NR060117) and the Korea Basic Science Institute (National Research Facilities and Equipment Center) grant funded by the Ministry of Education (2020R1A6C101A184).

Notes and references

1 S. Ji, B. Jiang, H. Hao, Y. Chen, J. Dong, Y. Mao, Z. Zhang, R. Gao, W. Chen, R. Zhang, Q. Liang, H. Li, S. Liu, Y. Wang, Q. Zhang, L. Gu, D. Duan, M. Liang, D. Wang, X. Yan and Y. Li, Matching the kinetics of natural enzymes with a single-atom iron nanozyme, *Nat. Catal.*, 2021, **4**, 407–417.
2 L. Shen, D. Ye, H. Zhao and J. Zhang, Perspectives for single-atom nanozymes: advanced synthesis, functional mechanisms, and biomedical applications, *Anal. Chem.*, 2020, **93**, 1221–1231.
3 Y. Huang, J. Ren and X. Qu, Nanozymes: classification, catalytic mechanisms, activity regulation, and applications, *Chem. Rev.*, 2019, **119**, 4357–4412.
4 Y. Zhang, G. Wei, W. Liu, T. Li, Y. Wang, M. Zhou, Y. Liu, X. Wang and H. Wei, Nanozymes for nanohealthcare, *Nat. Rev. Methods Primers*, 2024, **4**, 36.
5 Q. H. Nguyen and M. I. Kim, Using nanomaterials in colorimetric toxin detection, *BioChip J.*, 2021, **15**, 123–134.
6 F. Meng, P. Zhu, L. Yang, L. Xia and H. Liu, Nanozymes with atomically dispersed metal centers: structure–activity relationships and biomedical applications, *Chem. Eng. J.*, 2023, **452**, 139411.
7 B. Qiao, A. Wang, X. Yang, L. F. Allard, Z. Jiang, Y. Cui, J. Liu, J. Li and T. Zhang, Single-atom catalysis of CO oxidation using Pt1/FeO x, *Nat. Chem.*, 2011, **3**, 634–641.
8 L. Huang, J. Chen, L. Gan, J. Wang and S. Dong, Single-atom nanozymes, *Sci. Adv.*, 2019, **5**, eaav5490.
9 L. Jiao, H. Yan, Y. Wu, W. Gu, C. Zhu, D. Du and Y. Lin, When nanozymes meet single-atom catalysis, *Angew. Chem.*, 2020, **59**, 2565–2576.
10 Q. Wang, Y. Wu, Y. Mao and L. Zheng, Single-atom nanozymes: recent advances and perspectives toward application in food analysis, *Trends Food Sci. Technol.*, 2025, 104905.
11 W. Wu, L. Huang, E. Wang and S. Dong, Atomic engineering of single-atom nanozymes for enzyme-like catalysis, *Chem. Sci.*, 2020, **11**, 9741–9756.
12 X. Xiao, X. Hu, Q. Liu, Y. Zhang, G.-J. Zhang and S. Chen, Single-atom nanozymes as promising catalysts for biosensing and biomedical applications, *Inorg. Chem. Front.*, 2023, **10**, 4289–4312.
13 M. Maruthupandi and N. Y. Lee, Recent Advances in Electrochemical and Optical Point-of-Care Testing for Marine Biotoxin Detection, *BioChip J.*, 2025, 1–25.
14 J. Han, Y. Gu, C. Yang, L. Meng, R. Ding, Y. Wang, K. Shi and H. Yao, Single-atom nanozymes: classification, regulation strategy, and safety concerns, *J. Mater. Chem. B*, 2023, **11**, 9840–9866.
15 X. Cai, F. Ma, J. Jiang, X. Yang, Z. Zhang, Z. Jian, M. Liang, P. Li and L. Yu, Fe-NC single-atom nanozyme for ultrasensitive, on-site and multiplex detection of mycotoxins using lateral flow immunoassay, *J. Hazard. Mater.*, 2023, **441**, 129853.

16 Z. Lin, L. Zheng, W. Yao, S. Liu, Y. Bu, Q. Zeng, X. Zhang, H. Deng, X. Lin and W. Chen, A facile route for constructing Cu–N–C peroxidase mimics, *J. Mater. Chem. B*, 2020, **8**, 8599–8606.
17 G. Wu, S. Li, L. Luo, Y. Li, W. Zhang, H. Wang, S. Liu, C. Du, J. Wang and J. Cheng, Exploring Single-Atom Nanozymes Toward Environmental Pollutants: Monitoring and Control, *Nano-Micro Lett.*, 2025, **17**, 1–33.
18 X. Liu, B. Chen, J. Chen, X. Wang, X. Dai, Y. Li, H. Zhou, L. M. Wu, Z. Liu and Y. Yang, A cardiac-targeted nanozyme interrupts the inflammation-free radical cycle in myocardial infarction, *Adv. Mater.*, 2024, **36**, 2308477.
19 W. Qiao, J. Chen, H. Zhou, C. Hu, S. Dalangood, H. Li, D. Yang, Y. Yang and J. Gui, A single-atom manganese nanozyme Mn-N/C promotes anti-tumor immune response via eliciting type I interferon signaling, *Adv. Sci.*, 2024, **11**, 2305979.
20 Y. Jiang, Z. Chen, Y. Yuan, L. Tian, C. Dong, W. Shen, J. Wei, S. Wang, Y. Yang and J. Ge, Cu–N–C single-atom nanozyme as an ultrasensitive sensing platform for α-glucosidase detection, *Mater. Today Chem.*, 2024, **41**, 102327.
21 J. Ge, X. Sun, X. Li, Y. Yang, L. Zhang, L. Qu and Z. Li, Smartphone-assisted ultrasensitive colorimetric strategy based on Cu-CN single-atom nanozyme for acrylamide detection in fried food, *Food Chem.*, 2025, 145066.
22 J. Sun, M. Yan, G. Tao, R. Su, X. Xiao, Q. Wu, F. Chen, X.-L. Wu and H. Lin, A single-atom manganese nanozyme mediated membrane reactor for water decontamination, *Water Res.*, 2025, **268**, 122627.
23 V. Kandathil and S. A. Patil, Single-atom nanozymes and environmental catalysis: A perspective, *Adv. Colloid Interface Sci.*, 2021, **294**, 102485.
24 Z. Guo, J. Hong, N. Song and M. Liang, Single-atom nanozymes: from precisely engineering to extensive applications, *Acc. Mater. Res.*, 2024, **5**, 347–357.
25 J. Sun, Z. Wang and J. Guan, Single-atom nanozyme-based electrochemical sensors for health and food safety monitoring, *Food Chem.*, 2023, **425**, 136518.
26 Z. Lyu, J. Zhou, S. Ding, D. Du, J. Wang, Y. Liu and Y. Lin, Recent advances in single-atom nanozymes for colorimetric biosensing, *TrAC, Trends Anal. Chem.*, 2023, **168**, 117280.
27 F. Han, C. Cheng, J. Zhao, H. Wang, G. Zhao, Y. Zhang, N. Zhang, Y. Wang, J. Zhang and Q. Wei, Single-atom nanozymes: Emerging talent for sensitive detection of heavy metals, *Colloids Surf., B*, 2024, **242**, 114093.
28 S. Zhang, W. Ruan and J. Guan, Single-atom nanozymes for antibacterial applications, *Food Chem.*, 2024, **456**, 140094.
29 H. Zhang, X. F. Lu, Z.-P. Wu and X. W. D. Lou, Emerging multifunctional single-atom catalysts/nanozymes, *ACS Cent. Sci.*, 2020, **6**, 1288–1301.
30 M. S. Kim, J. Lee, H. S. Kim, A. Cho, K. H. Shim, T. N. Le, S. S. A. An, J. W. Han, M. I. Kim and J. Lee, Heme cofactor-resembling Fe–N single site embedded graphene as nanozymes to selectively detect H2O2 with high sensitivity, *Adv. Funct. Mater.*, 2020, **30**, 1905410.
31 Y. Wu, L. Jiao, X. Luo, W. Xu, X. Wei, H. Wang, H. Yan, W. Gu, B. Z. Xu and D. Du, Oxidase-like Fe-N-C single-atom nanozymes for the detection of acetylcholinesterase activity, *Small*, 2019, **15**, 1903108.
32 S. Sun, G. Zhang, N. Gauquelin, N. Chen, J. Zhou, S. Yang, W. Chen, X. Meng, D. Geng and M. N. Banis, Single-atom catalysis using Pt/graphene achieved through atomic layer deposition, *Sci. Rep.*, 2013, **3**, 1775.
33 L. Zhou, X. Chang, W. Zheng, X. Liu and J. Zhang, Single atom Rh-sensitized SnO2 via atomic layer deposition for efficient formaldehyde detection, *Chem. Eng. J.*, 2023, **475**, 146300.
34 T. Li, J. Liu, Y. Song and F. Wang, Photochemical solid-phase synthesis of platinum single atoms on nitrogen-doped carbon with high loading as bifunctional catalysts for hydrogen evolution and oxygen reduction reactions, *ACS Catal.*, 2018, **8**, 8450–8458.
35 H. Wei, K. Huang, D. Wang, R. Zhang, B. Ge, J. Ma, B. Wen, S. Zhang, Q. Li and M. Lei, Iced photochemical reduction to synthesize atomically dispersed metals by suppressing nanocrystal growth, *Nat. Commun.*, 2017, **8**, 1490.
36 T. Gan, Q. He, H. Zhang, H. Xiao, Y. Liu, Y. Zhang, X. He and H. Ji, Unveiling the kilogram-scale gold single-atom catalysts via ball milling for preferential oxidation of CO in excess hydrogen, *Chem. Eng. J.*, 2020, **389**, 124490.
37 H. Xu, L. Zhang, H. Wang, S. Zhang, W. Li, X. Wang, S. Song, D. Wang and Z. Shi, Ball-milling Synthesis of Single-atom Cu Anchored on N-Doped Carbon for Mimicking Peroxidase, *Chem. Res. Chin. Univ.*, 2023, **39**, 948–953.
38 U. Heiz, A. Sanchez, S. Abbet and W.-D. Schneider, Catalytic oxidation of carbon monoxide on monodispersed platinum clusters: each atom counts, *J. Am. Chem. Soc.*, 1999, **121**, 3214–3217.
39 G. Kwon, G. A. Ferguson, C. J. Heard, E. C. Tyo, C. Yin, J. DeBartolo, S. n. Seifert, R. E. Winans, A. J. Kropf and J. Greeley, Size-dependent subnanometer Pd cluster (Pd4, Pd6, and Pd17) water oxidation electrocatalysis, *ACS Nano*, 2013, **7**, 5808–5817.
40 Y. Fan, Y. Yi, H. Rong and J. Zhang, Silicon dioxide-protection boosting the peroxidase-like activity of Fe single-atom catalyst for combining chemo-photothermal therapy, *Nano Res.*, 2024, **17**, 4924–4933.
41 Q. Wang, Y. Yang, F. Sun, G. Chen, J. Wang, L. Peng, W. T. Chen, L. Shang, J. Zhao and D. Sun-Waterhouse, Molten NaCl-assisted synthesis of porous Fe-N-C electrocatalysts with a high density of catalytically accessible FeN4 active sites and outstanding oxygen reduction reaction performance, *Adv. Energy Mater.*, 2021, **11**, 2100219.
42 W. Liu, L. Zhang, W. Yan, X. Liu, X. Yang, S. Miao, W. Wang, A. Wang and T. Zhang, Single-atom dispersed Co–N–C catalyst: structure identification and performance for hydrogenative coupling of nitroarenes, *Chem. Sci.*, 2016, **7**, 5758–5764.
43 C.-N. Zhu, X. Chen, Y.-Q. Xu, F. Wang, D.-Y. Zheng, C. Liu, X.-H. Zhang, Y. Yi and D.-B. Cheng, Advanced Preparation Methods and Biomedical Applications of Single-Atom Nanozymes, *ACS Biomater. Sci. Eng.*, 2024, **10**, 7352–7371.

44 X. Lu, S. Gao, H. Lin, L. Yu, Y. Han, P. Zhu, W. Bao, H. Yao, Y. Chen and J. Shi, Bioinspired copper single-atom catalysts for tumor parallel catalytic therapy, *Adv. Mater.*, 2020, **32**, 2002246.
45 X. Chen, L. Luo, Y. Zhang and X. Zhao, Theoretical screening of highly efficient single-atom catalysts based on covalent triazine frameworks for oxygen reduction, *Langmuir*, 2023, **39**, 6905–6913.
46 Y. Shang, X. Xu, B. Gao, S. Wang and X. Duan, Single-atom catalysis in advanced oxidation processes for environmental remediation, *Chem. Soc. Rev.*, 2021, **50**, 5281–5322.
47 C. A. Jhabvala, P. C. Nagler and T. R. Stevenson, Atomic Layer Deposition Josephson Junctions for Cryogenic Circuit Applications, *J. Low Temp. Phys.*, 2020, **200**, 331–335.
48 C. H. Choi, M. Kim, H. C. Kwon, S. J. Cho, S. Yun, H.-T. Kim, K. J. Mayrhofer, H. Kim and M. Choi, Tuning selectivity of electrochemical reactions by atomically dispersed platinum catalyst, *Nat. Commun.*, 2016, **7**, 10922.
49 N. Cheng, J. C. Li, D. Liu, Y. Lin and D. Du, Single-atom nanozyme based on nanoengineered Fe–N–C catalyst with superior peroxidase-like activity for ultrasensitive bioassays, *Small*, 2019, **15**, 1901485.
50 J. Li, Q. Guan, H. Wu, W. Liu, Y. Lin, Z. Sun, X. Ye, X. Zheng, H. Pan and J. Zhu, Highly active and stable metal single-atom catalysts achieved by strong electronic metal–support interactions, *J. Am. Chem. Soc.*, 2019, **141**, 14515–14519.
51 Y. Wang, K. Qi, S. Yu, G. Jia, Z. Cheng, L. Zheng, Q. Wu, Q. Bao, Q. Wang and J. Zhao, Revealing the intrinsic peroxidase-like catalytic mechanism of heterogeneous single-atom Co–MoS2, *Nano-Micro Lett.*, 2019, **11**, 102.
52 S. Ding, J. A. Barr, Z. Lyu, F. Zhang, M. Wang, P. Tieu, X. Li, M. H. Engelhard, Z. Feng and S. P. Beckman, Effect of phosphorus modulation in iron single-atom catalysts for peroxidase mimicking, *Adv. Mater.*, 2024, **36**, 2209633.
53 L. Jiao, W. Xu, Y. Zhang, Y. Wu, W. Gu, X. Ge, B. Chen, C. Zhu and S. Guo, Boron-doped Fe-NC single-atom nanozymes specifically boost peroxidase-like activity, *Nano Today*, 2020, **35**, 100971.
54 Y. Chen, G. Li, Y. Zeng, L. Yan, X. Wang, L. Yang, Q. Wu and Z. Hu, Boosting faradaic efficiency of CO2 electroreduction to CO for Fe− N− C single-site catalysts by stabilizing Fe3+ sites via F-doping, *Nano Res.*, 2022, **15**, 7896–7902.
55 B. Xu, S. Li, L. Zheng, Y. Liu, A. Han, J. Zhang, Z. Huang, H. Xie, K. Fan and L. Gao, A bioinspired five-coordinated single-atom iron nanozyme for tumor catalytic therapy, *Adv. Mater.*, 2022, **34**, 2107088.
56 W. Ma, J. Mao, X. Yang, C. Pan, W. Chen, M. Wang, P. Yu, L. Mao and Y. Li, A single-atom Fe–N 4 catalytic site mimicking bifunctional antioxidative enzymes for oxidative stress cytoprotection, *Chem. Commun.*, 2019, **55**, 159–162.
57 X. Sun, C. Chen, C. Xiong, C. Zhang, X. Zheng, J. Wang, X. Gao, Z.-Q. Yu and Y. Wu, Surface modification of MoS2 nanosheets by single Ni atom for ultrasensitive dopamine detection, *Nano Res.*, 2023, **16**, 917–924.
58 Y. Wang, J. Wu, S. Tang, J. Yang, C. Ye, J. Chen, Y. Lei and D. Wang, Synergistic Fe− Se atom pairs as bifunctional oxygen electrocatalysts boost low-temperature rechargeable Zn-air battery, *Angew. Chem.*, 2023, **62**, e202219191.
59 Y. Hu, T. Chao, Y. Li, P. Liu, T. Zhao, G. Yu, C. Chen, X. Liang, H. Jin and S. Niu, Cooperative Ni (Co)-Ru-P sites activate dehydrogenation for hydrazine oxidation assisting self-powered H2 production, *Angew. Chem.*, 2023, **62**, e202308800.
60 J. Shen, J. Chen, Y. Qian, X. Wang, D. Wang, H. Pan and Y. Wang, Atomic engineering of single-atom nanozymes for biomedical applications, *Adv. Mater.*, 2024, **36**, 2313406.
61 Y. Xu, C. Dong, X. Liu, D. Wei, Z. Chen, H. Zhou, J. b. Li, Y. Yang and W. Tan, Single-Atom Enzymes: From Evolutionary Insights, Precision Engineering to Breakthroughs in Biomedical Applications, *Small*, 2025, e05750.
62 Y. Li, X. Zhu, L. Li, F. Li, X. Zhang, Y. Li and Z. Zheng, Study on the structure-activity relationship between single-atom, cluster and nanoparticle catalysts in a hierarchical structure for the oxygen reduction reaction, *Small*, 2022, **18**, 2105487.
63 S. Wu, J. Xia, R. Li, H. Cao and D. Ye, Perspectives for the role of single-atom nanozymes in assisting food safety inspection and food nutrition evaluation, *Anal. Chem.*, 2024, **96**, 1813–1824.
64 L. Jiao, J. Wu, H. Zhong, Y. Zhang, W. Xu, Y. Wu, Y. Chen, H. Yan, Q. Zhang, W. Gu, L. Gu, S. P. Beckman, L. Huang and C. Zhu, Densely Isolated FeN4 Sites for Peroxidase Mimicking, *ACS Catal.*, 2020, **10**, 6422–6429.
65 Y. Chen, P. Wang, H. Hao, J. Hong, H. Li, S. Ji, A. Li, R. Gao, J. Dong, X. Han, M. Liang, D. Wang and Y. Li, Thermal Atomization of Platinum Nanoparticles into Single Atoms: An Effective Strategy for Engineering High-Performance Nanozymes, *J. Am. Chem. Soc.*, 2021, **143**, 18643–18651.
66 Z. Lyu, S. Ding, N. Zhang, Y. Zhou, N. Cheng, M. Wang, M. Xu, Z. Feng, X. Niu and Y. Cheng, Single-atom nanozymes linked immunosorbent assay for sensitive detection of Aβ 1-40: a biomarker of Alzheimer's disease, *Research*, 2020, **2020**, 4724505.
67 P. Xu, C. Tao, Y. Jiang, S. Chu, K. Song and Y. Lu, Concave single-atom Co nanozymes with densely edge-hosted active sites for highly sensitive immunoassay, *Chem. Eng. J.*, 2024, **495**, 153479.
68 Y. Huang, Q. Shen, Y. Pu, J. Yu, Y. Xiong, T. Gan, L. Tao, J. Zhang and X. Huang, Promotion of Single-Electron Transfer by Low-Coordinated Co Single Atoms to Facilitate Advanced Oxidation Processes in Wastewater Treatment, *Inorg. Chem.*, 2024, **63**, 21567–21576.
69 S. Lee, H.-S. Bae and W. Choi, Selective Control and Characteristics of Water Oxidation and Dioxygen Reduction in Environmental Photo(electro)catalytic Systems, *Acc. Chem. Res.*, 2023, **56**, 867–877.
70 Y. Dong, W. Peng, Y. Liu and Z. Wang, Photochemical origin of reactive radicals and halogenated organic substances in natural waters: A review, *J. Hazard. Mater.*, 2021, **401**, 123884.

71 Q.-Y. Wu, Z.-W. Yang, Z.-W. Wang and W.-L. Wang, Oxygen doping of cobalt-single-atom coordination enhances peroxymonosulfate activation and high-valent cobalt–oxo species formation, *Proc. Natl. Acad. Sci. U. S. A.*, 2023, **120**, e2219923120.

72 R. O. Saleh, E. A. M. Saleh, M. Moharam, S. Uthirapathy, S. Ballal, A. Singh, A. Nanda, S. Ray, A. K. Nasir and R. S. Kaurshead, Recent trends and advances in single-atom nanozymes for the electrochemical and optical sensing of pesticide residues in food and water, *RSC Adv.*, 2025, **15**, 15919–15939.

73 X. Niu, Q. Shi, W. Zhu, D. Liu, H. Tian, S. Fu, N. Cheng, S. Li, J. N. Smith, D. Du and Y. Lin, Unprecedented peroxidase-mimicking activity of single-atom nanozyme with atomically dispersed Fe–Nx moieties hosted by MOF derived porous carbon, *Biosens. Bioelectron.*, 2019, **142**, 111495.

74 M. Wang, L. Liu, X. Xie, X. Zhou, Z. Lin and X. Su, Single-atom iron containing nanozyme with peroxidase-like activity and copper nanoclusters based ratio fluorescent strategy for acetylcholinesterase activity sensing, *Sens. Actuators, B*, 2020, **313**, 128023.

75 Y. Wang, G. Jia, X. Cui, X. Zhao, Q. Zhang, L. Gu, L. Zheng, L. H. Li, Q. Wu, D. J. Singh, D. Matsumura, T. Tsuji, Y.-T. Cui, J. Zhao and W. Zheng, Coordination Number Regulation of Molybdenum Single-Atom Nanozyme Peroxidase-like Specificity, *Chem*, 2021, **7**, 436–449.

76 J. Yang, R. Zhang, H. Zhao, H. Qi, J. Li, J.-F. Li, X. Zhou, A. Wang, K. Fan, X. Yan and T. Zhang, Bioinspired copper single-atom nanozyme as a superoxide dismutase-like antioxidant for sepsis treatment, *Exploration*, 2022, **2**, 20210267.

77 E. M. Hamed, F. M. Fung and S. F. Y. Li, Bimetallic Cu/Zn Single-Atom Nanozyme with Superoxide Dismutase-Like Activity, *Small*, 2025, **21**, e03879.

78 J. Ge, L. Yang, Z. Li, Y. Wan, D. Mao, R. Deng, Q. Zhou, Y. Yang and W. Tan, A colorimetric smartphone-based platform for pesticides detection using Fe-N/C single-atom nanozyme as oxidase mimetics, *J. Hazard. Mater.*, 2022, **436**, 129199.

79 Y. Han, X. Tang, X. Wu, H. Shi, L. Huang, L. Wei, M. Li and Y. Zhang, Single-atom Co-N-C nanozymes with excellent oxidase-like activity for colorimetric detection of l-cysteine, *Spectrochim. Acta, Part A*, 2025, **332**, 125778.

80 D. Xu, F. Yang, Y. Ou, Q. Pu, Q. Chen, H. Pei, B. Huang, Q. Wu and Y. Wang, Highly accessible Fe–N–C single-atom nanozymes with enhanced oxidase-like activity for smartphone-assisted colorimetric detection of uric acid, *Talanta*, 2025, **293**, 128076.

81 S. Li, F. Wang, C. Wang, L. Hao, N. Shang, P. Zhang, Y. Zhang, N. Xiao, Y. Kang, J. Liu, S. Gao, C. Wang, Z. Wang and Q. Wu, B Doped Zn Single-Atom Nanozyme With Enhanced Oxidase-Like Activity Combined CRISPR/Cas13a System for RNA Sensing, *Adv. Funct. Mater.*, 2025, **35**, 2418523.

82 H. Ruan, S. Zhang, H. Wang, J. Pei, R. Zhao, X. Mu, H. Wang and X. Zhang, Single-Atom Pd/CeO2 Nanostructures for Mimicking Multienzyme Activities, *ACS Appl. Nano Mater.*, 2022, **5**, 6564–6574.

83 J. Zhong, X. Yang, S. Gao, J. Luo, J. Xiang, G. Li, Y. Liang, L. Tang, C. Qian, J. Zhou, L. Zheng, K. Zhang and J. Zhao, Geometric and Electronic Structure-Matched Superoxide Dismutase-Like and Catalase-Like Sequential Single-Atom Nanozymes for Osteoarthritis Recession, *Adv. Funct. Mater.*, 2023, **33**, 2209399.

84 J. Xu, M. Zhang, H. Song and W. Tong, A platinum nanoparticles-loaded copper single-atom nanozymes cascade platform for efficient ROS scavenging: structure-activity optimization and kinetic visualization via simulation, *Colloids Surf., A*, 2025, **726**, 138056.

85 R. Wang, X. Ma, E. M. Hamed, B. Cao, L. Wang, S. F. Y. Li and Y. Zhu, Deciphering of laccase-like activity ruthenium single-atom nanozyme for identification/quantification and remediation of phenolic pollutants, *Sens. Actuators, B*, 2025, **426**, 137112.

86 Y. Mao, S. Gao, L. Yao, L. Wang, H. Qu, Y. Wu, Y. Chen and L. Zheng, Single-atom nanozyme enabled fast and highly sensitive colorimetric detection of Cr(VI), *J. Hazard. Mater.*, 2021, **408**, 124898.

87 R. Li, X. He, R. Javed, J. Cai, H. Cao, X. Liu, Q. Chen, D. Ye and H. Zhao, Switching on-off-on colorimetric sensor based on Fe-N/S-C single-atom nanozyme for ultrasensitive and multimodal detection of Hg^{2+}, *Sci. Total Environ.*, 2022, **834**, 155428.

88 G. Song, J.-C. Li, Z. Majid, W. Xu, X. He, Z. Yao, Y. Luo, K. Huang and N. Cheng, Phosphatase-like activity of single-atom CeNC nanozyme for rapid detection of Al^{3+}, *Food Chem.*, 2022, **390**, 133127.

89 G. Song, Q. Zhang, S. Liang, Y. Yao, M. Feng, Z. Majid, X. He, K. Huang, J.-C. Li and N. Cheng, Oxidation activity modulation of a single atom Ce-NC nanozyme enabling a time-resolved sensor to detect Fe $^{3+}$ and Cr $^{6+}$, *J. Mater. Chem. C*, 2022, **10**, 15656–15663.

90 T. Li, J. Xia, M. Wu, C. Liu, Y. Sun, W. Zhao, M. Qian, W. Wang, W. Duan and S. Xu, Single-Atom Iridium-doped Carbon Dots Nanozyme with High Peroxidase-Like Activity as Colorimetric Sensors for Multimodal Detection of Mercury Ions, *Small*, 2025, 2408785.

91 L. Yao, S. Gao, S. Liu, Y. Bi, R. Wang, H. Qu, Y. Wu, Y. Mao and L. Zheng, Single-Atom Enzyme-Functionalized Solution-Gated Graphene Transistor for Real-Time Detection of Mercury Ion, *ACS Appl. Mater. Interfaces*, 2020, **12**, 6268–6275.

92 S. Chu, M. Xia, P. Xu, D. Lin, Y. Jiang and Y. Lu, Single-atom Fe nanozymes with excellent oxidase-like and laccase-like activity for colorimetric detection of ascorbic acid and hydroquinone, *Anal. Bioanal. Chem.*, 2024, **416**, 6067–6077.

93 B. Liu, Z. Wang, T. Wei, Z. Liu and J. Li, Bimetallic FeMn-N nanoparticles as nanocatalyst with dual enzyme-mimic activities for simultaneous colorimetric detection and degradation of hydroquinone, *J. Environ. Chem. Eng.*, 2023, **11**, 110186.

94 Y. Lin, F. Wang, J. Yu, X. Zhang and G.-P. Lu, Iron single-atom anchored N-doped carbon as a 'laccase-like' nanozyme for the degradation and detection of phenolic pollutants and adrenaline, *J. Hazard. Mater.*, 2022, **425**, 127763.
95 J. Xia, R. Fu, Z. Li, Y. Ding, H. Zhao and D. Ye, Graphyne-supported manganese single-atom nanozyme sensor array for bisphenol identification, *Talanta*, 2025, **285**, 127326.
96 G. Song, Z. Zhang, M.-L. Fauconnier, C. Li, L. Chen, X. Zheng and D. Zhang, Bimodal single-atom iron nanozyme biosensor for volatile amine and food freshness detection, *Nano Today*, 2023, **53**, 102025.
97 D. Zhang, D. Kukkar, H. Kaur and K.-H. Kim, Recent advances in the synthesis and applications of single-atom nanozymes in food safety monitoring, *Adv. Colloid Interface Sci.*, 2023, **319**, 102968.
98 X. Wang, Q. Sun, J. Yu, J. Sun, N. Niu and L. Chen, Lignin-based iron single-atom nanozyme for detection of organophosphorus in soil, *Microchem. J.*, 2023, **195**, 109381.
99 Z. Zhao, X. Shi, Z. Shen, Y. Gu, L. He, M. Zhang and N. Lu, Single-atom Fe nanozymes coupling with atomic clusters as superior oxidase mimics for ratiometric fluorescence detection, *Chem. Eng. J.*, 2023, **469**, 143923.
100 Z. Lyu, S. Ding, P. Tieu, L. Fang, X. Li, T. Li, X. Pan, M. H. Engelhard, X. Ruan, D. Du, S. Li and Y. Lin, Single-Atomic Site Catalyst Enhanced Lateral Flow Immunoassay for Point-of-Care Detection of Herbicide, *Research*, 2022, **2022**, 9823290.
101 G. Wang, J. Liu, H. Dong, L. Geng, J. Sun, J. Liu, J. Dong, Y. Guo and X. Sun, A dual-mode biosensor featuring single-atom Fe nanozyme for multi-pesticide detection in vegetables, *Food Chem.*, 2024, **437**, 137882.
102 L. Zhang, Z. Lang, B. Lu, T. Yang, X. Zhang, M. Wang, X. Zhang, H. Cao and D. Ye, Smartphone-based colorimetric paper chip sensor using single-atom nanozyme for the detection of carbofuran pesticide residues in vegetables, *Spectrochim. Acta, Part A*, 2025, **327**, 125415.
103 X. Xu, M. Ma, J. Gao, T. Sun, Y. Guo, D. Feng and L. Zhang, Multifunctional Ni-NPC Single-Atom Nanozyme for Removal and Smartphone-Assisted Visualization Monitoring of Carbamate Pesticides, *Inorg. Chem.*, 2024, **63**, 1225–1235.
104 Y. Fan, X. Gan, H. Zhao, Z. Zeng, W. You and X. Quan, Multiple application of SAzyme based on carbon nitride nanorod-supported Pt single-atom for H_2O_2 detection, antibiotic detection and antibacterial therapy, *Chem. Eng. J.*, 2022, **427**, 131572.
105 R. Huang, T. T. Zigale, H. Meng, L. Wang, Q. Dong, K. Zeng and Z. Zhang, Cobalt Single-Atom Nanozyme-Enabled Multimodal Lateral Flow Immunoassay for On-Site Ultrasensitive Detection of Tetracycline Residues in Agri-Food Products, *J. Agric. Food Chem.*, 2025, **73**, 16648–16659.
106 F. Yu, M. Huang, R. Wang, C. Hao and Y. Zhu, Single-atom ruthenium nanozyme-induced signal amplification strategy in photoelectrochemical aptasensor for ultrasensitive detection of chloramphenicol, *Biosens. Bioelectron.*, 2025, **268**, 116917.
107 X. Xie, Y. Zhao, Y. Fan, L. Jiang, W. Liu and X. Yang, Multifunctional Fe/Cu Dual-Single Atom Nanozymes with Enhanced Peroxidase Activity for Isoniazid Detection and Levofloxacin Degradation, *Langmuir*, 2024, **40**, 12671–12680.
108 A. S. Sharma, J. H. Lee, S. M. Ryou and N. Y. Lee, Nucleic acid-templated toluidine blue O assemblies as colorimetric probes for point-of-care nucleic acid tests, *Int. J. Biol. Macromol.*, 2025, 144765.
109 M. Feng, Q. Zhang, X. Chen, D. Deng, X. Xie and X. Yang, Controllable synthesis of boron-doped Zn–N–C single-atom nanozymes for the ultrasensitive colorimetric detection of p-phenylenediamine, *Biosens. Bioelectron.*, 2022, **210**, 114294.
110 Q. Feng, G. Wang, L. Xue, Y. Wang, M. Liu, J. Liu, S. Zhang and W. Hu, Single-Atom Nanozyme Based on Mn-Center with Enhanced Peroxidase-like Activity for Organic Dye Degradation, *ACS Appl. Nano Mater.*, 2023, **6**, 4844–4853.
111 G. Ning, H. Liang, L. Guo, X. Lu, L. Xiao, T. Qi, H. Zhao and C.-P. Li, Chiral FeNC single-atom nanozymes with multi-enzyme activity for dye degradation, *J. Environ. Chem. Eng.*, 2024, **12**, 114471.
112 Q. Chen, Y. Liu, Y. Lu, Y. Hou, X. Zhang, W. Shi and Y. Huang, Atomically dispersed Fe/Bi dual active sites single-atom nanozymes for cascade catalysis and peroxymonosulfate activation to degrade dyes, *J. Hazard. Mater.*, 2022, **422**, 126929.
113 S. Wu, W. Wu, X. Zhu, M. Li, J. Zhao and S. Dong, Atomically dispersed hierarchically ordered porous Fe-N-C single-atom nanozymes for dyes degradation, *Nano Res.*, 2023, **16**, 10840–10847.
114 A. Selva Sharma and N. Y. Lee, Advancements in visualizing loop-mediated isothermal amplification (LAMP) reactions: A comprehensive review of colorimetric and fluorometric detection strategies for precise diagnosis of infectious diseases, *Coord. Chem. Rev.*, 2024, **509**, 215769.
115 X. Dai, H. Liu, B. Cai, Y. Liu, K. Song, J. Chen, S. Q. Ni, L. Kong and J. Zhan, A Bioinspired Atomically Thin Nanodot Supported Single-Atom Nanozyme for Antibacterial Textile Coating, *Small*, 2023, **19**, 2303901.
116 C. Huang, F. Xu, Z. Huang, L. Hao, X. Wu, T. Ye, M. Yuan, J. Yu, F. Yin and H. Cao, Iron–Copper Single-Atom Nanozyme for Enhanced Synergistic Antibacterial Activity, *ACS Appl. Nano Mater.*, 2025, **8**, 7887–7898.
117 F. Wu, Y. Wang, Y. Li, L. Shi, L. Yuan, Y. Ren, H. C. van der Mei and Y. Liu, Single-Atom Cu Anchored on Carbon Nitride as a Bifunctional Glucose Oxidase and Peroxidase Nanozyme for Antibacterial Therapy, *ACS Nano*, 2025, **19**, 10816–10828.
118 Z. Shen, P. Wang, X. Li, M. Zhang, X. Shi and N. Lu, Heteroatom-regulated iron single-atom nanozymes for universal colorimetric discrimination of mycotoxins and metal ions, *Chem. Eng. J.*, 2024, **502**, 157902.
119 Y. Zhang, H. Lin, L. Wang, L. He, Y. Man, B. Jia, Z. Yan, S. Kang, H. Xie and A. Wu, Modulating the electronic

configuration of single-atom nanozymes using cobalt nanoclusters for enhanced mycotoxin degradation, *Food Chem.*, 2025, **479**, 143852.
120 M. Liu, X. Li, S. Zhou, D. Men, Y. Duan, H. Liu, B. Zhao, D. Huo and C. Hou, Ultrasensitive detection of mycotoxins using a novel single-Atom, CRISPR/Cas12a-Based nanozymatic colorimetric biosensor, *Chem. Eng. J.*, 2024, **497**, 154418.
121 Z. Han, D. Tranca, F. Rodríguez-Hernández, K. Jiang, J. Zhang, M. He, F. Wang, S. Han, P. Wu and X. Zhuang, Embedding Ru clusters and single atoms into perovskite oxide boosts nitrogen fixation and affords ultrahigh ammonia yield rate, *Small*, 2023, **19**, 2208102.
122 N. Goyal, F. Li and Y.-b. Hu, Tailoring single-metal atom catalysts: a strategic defect engineering approach for electrochemical reduction reactions, *J. Mater. Chem. A*, 2024, **12**, 19685–19719.
123 L. He, C. Guan, D. A. Bulushev and Q. Xiang, Regulation of Metal-Support Interaction in Single-Atom Catalysis, *Small*, 2024, 2410976.